



universität
wien

MASTERARBEIT

Titel der Masterarbeit

„Characterization of a novel zebrafish mutant
defective in retinal pigment epithelium maintenance “

verfasst von

Marion Claudia Salzer BSc

angestrebter akademischer Grad

Master of Science (MSc)

Wien, 2013

Studienkennzahl lt.
Studienblatt:

A 066 877

Studienrichtung lt.
Studienblatt:

Masterstudiengang „Genetik und Entwicklungsbiologie“

Betreut von:

Dr. Florian Raible

Table of Contents

1. Abstract	3
2. Introduction	5
2.1 Preface	5
2.2 Zebrafish eye development.....	6
2.2.1 The neural retina.....	6
2.2.2 The retinal pigment epithelium (RPE).....	7
2.3 The cardiovascular system in zebrafish	8
2.3.1 Development of the vascular tree	8
2.3.2 Vascular development in the zebrafish eye	9
2.3.3 Structural differences between vessels.....	10
2.3.4 Regulation of endothelial permeability.....	11
2.4 Barriers in the brain and retina	13
2.4.1 Neuroepithelial-ventricular barrier in the embryo	14
2.4.2 The blood-CSF barrier in the adult.....	14
2.4.3 Blood-brain barrier (BBB).....	15
2.4.4 Blood-retina barrier (BRB).....	16
2.5 Aims of this work	17
3. Results	19
3.1 The <i>modern art</i> mutant displays degeneration of various tissues, including the brain and retina.....	19
3.2 Early eye development is not affected in <i>moda</i> mutants, but the dorsal retina starts to degenerate at 2 dpf.....	21
3.3 Actively migrating retinal pigment epithelium cell clusters co-localize with the macrophage specific marker L-plastin.....	24
3.4 The <i>moda</i> mutation causes extensive apoptosis in the brain, eye, tail and fins	27
3.5 Extensive cell death in <i>moda</i> mutants is not caused by oxidative damage	28
3.6 Cell death and disruption of retinal organization is caused by a non-cell autonomous mechanism	29
3.7 The brain stops developing at 2 dpf and shows morphological defects in the embryonic ependyma	30
3.8 Cell death in the brain and retina is rescued by a loss of blood flow	31
3.9 The <i>moda</i> mutation lies in a maternal effect gene	35
3.10 The <i>moda</i> mutation maps to a 1.4Mb region on chromosome 16	37

4. Discussion	39
4.1 Cell death in the dorsal anterior brain and retina is likely caused by CSF that has leaked through the embryonic ependyma.....	39
4.2 Possible mechanisms that may lead to CNS degeneration in <i>moda</i> mutants..	41
4.2.1 Model 1: Increased endothelial permeability impairs ependymal function	41
4.2.2 Model 2: The <i>moda</i> mutation directly affects ependymal function	42
4.2.3 Model 3: The <i>moda</i> mutation mainly affects highly proliferating tissues due to early depletion of the maternal effect component.....	43
4.3 Similarities between the ventricle and the otic vesicle defect – requirement for ion channel regulation	45
4.4 The mutant locus maps to the upper arm of Chromosome 16	45
4.5 Future directions	49
5. Materials and Methods	51
5.1 ENU mutagenesis and zebrafish strains	51
5.2 Wholemount in situ hybridization.....	53
5.3 Wholemount antibody staining	56
5.4 TUNEL staining.....	57
5.5 Inhibition of Apoptosis	57
5.6 BrdU staining.....	57
5.7 Cell transplantation experiments	58
5.8 JB-4 sections	59
5.9 Alcain blue staining.....	59
5.10 β -Galactosidase-assay.....	59
5.11 Mapping the <i>moda</i> mutation	59
5.12 DIC time lapse imaging	60
5.13 Imaging and data processing	60
6. References	61
7. Annex 1: Supplementary Figures.....	69
8. Annex 2: Additional observations.....	77
9. Curriculum vitae.....	79
10. Abstract/Zusammenfassung	81
10.1. Abstract	81
10.2 Zusammenfassung.....	82
11. Acknowledgements	83

1. Abstract

Congenital eye diseases are among the leading causes of blindness in developed countries. A small number of blinding diseases are caused by defects in eye development; a comparably large number are caused by defects in functional maintenance of the retina.

With the aim to identify new factors that are implicated in the maintenance of retinal integrity and function, we performed an ENU mutagenesis screen in zebrafish and isolated one homozygous mutant that exhibits severe retinal degeneration during late embryonic development. I termed this mutant *modern art (moda)*. Retinal degeneration in *moda* mutants sets in at the level of the retinal pigment epithelium, a non-neural cell layer supporting the outer neural retina. Interestingly, rather than causing uniform cell death across the entire retinal tissue, the *moda* mutation leads to progressive neuronal loss primarily in the dorsal anterior quadrant of the eye.

Moda mutants display a variety of additional phenotypes. These include central nervous system (CNS) degeneration, whereby cell death starts at the ventricles and progressively spreads towards adjacent brain regions, and vascular abnormalities, which manifest in increased hemorrhaging in the CNS.

My results establish that retinal degeneration in *moda* mutants is caused by cell-extrinsic factors and that the manifestation of this phenotype is dependent on blood circulation. The mutant locus maps to a 1.4 Mb region on the left arm of Chr 16, which contains 24 candidate genes. Furthermore, I discovered that the *moda* mutation lies in a maternal effect gene. Based on my current results I suggest that cell death in the retina and CNS is caused by a disrupted neuroepithelial-ventricular barrier. Hopefully, investigation of this mutant will identify a new mechanism relevant for the pathogenesis of distinct neurodegenerative diseases in humans.

2. Introduction

2.1 Preface

Congenital eye diseases are among the leading causes of blindness in developed countries. A small number of blinding diseases are caused by defects in eye development; a comparably large number are caused by defects in functional maintenance of the retina. While developmental eye diseases result in a continuous visual impairment throughout life of the affected person, degenerative eye diseases manifest during adolescence or adulthood and lead to a progressive loss of vision. All degenerative eye diseases that have been described so far involve a gradual loss of light detecting photoreceptors and are therefore known as photoreceptor cell dystrophies. Both homozygous and heterozygous mutations of functionally diverse genes have been associated with this type of eye disease^[1].

Zebrafish has become an important model organism to study retinal diseases in vivo. Many mutant strains exhibiting photoreceptor degeneration during larval stages have been isolated and this has improved our understanding of the molecular and cellular mechanisms underlying these conditions^[1, 2].

With the aim to identify new factors that are implicated in the maintenance of retinal integrity and function, we performed an ENU mutagenesis screen in zebrafish and isolated one homozygous mutant that exhibits retinal degeneration during late embryonic development. I termed this mutant *modern art (moda)*. Retinal degeneration in *moda* mutants sets in at the level of the retinal pigment epithelium, a non-neural cell layer supporting the outer neural retina. Surprisingly, retinal degeneration is asymmetric across the retina, such that retinal cells located in the dorsal anterior quadrant of the eye are affected earliest and most severely. While in known retinal dystrophies degeneration sets in either in the peripheral retina or the central retina, the onset of degeneration in a defined sub-region has, to my knowledge, not been described.

The *moda* phenotype is not confined to retinal degeneration and a variety of additional defects can be observed in *moda* mutants. These include defects in fin and jaw development, otic vesicle collapse, central nervous system (CNS) degeneration and vascular abnormalities. Given our main interest in degenerative diseases of the eye, my investigation focuses on the cellular cause for retinal degeneration in *moda* mutants.

2.2 Zebrafish eye development

The vertebrate retina is a highly conserved structure. The two retinas develop from two bilateral evaginations of the forebrain neuroepithelium called optic vesicles. The distal portion of the optic vesicle invaginates to form the optic cup. During this process the choroid fissure is formed along the ventral retina and optic stalk, providing a path for retinal axons to exit and extra-ocular cells to enter the optic cup. The optic cup consists of two neuroepithelial layers. The inner layer forms the neural retina and the outer layer the retinal pigment epithelium (RPE). Development of the neural retina and the retinal pigment epithelium strongly depends on interaction between those two. Concomitantly, the lens placode, specified by the optic cup, forms from delaminating surface ectoderm and itself then induces the overlying ectoderm to form the cornea^[1, 3]. Eye development is influenced by reciprocal signaling interactions with the neighboring surface ectoderm, the ventral forebrain and the peri-ocular mesenchyme (POM), which consists of mesodermal and neuroectodermal cell populations. The POM plays an essential role during eye morphogenesis and contributes to the formation of the inner retinal vasculature and non-neural retinal tissues^[2].

2.2.1 The neural retina

All vertebrates have a three layered neural retina consisting, inside to outside, of the retinal ganglion cell layer, formed by neurons projecting to the contralateral optic tectum in the brain, the inner nuclear layer, formed by cell bodies of processing neurons, and the outer nuclear layer, formed by rod and cone photoreceptors (Fig.1). In zebrafish, the different cell classes are generated sequentially, with the retinal ganglion cells being produced between 24 and 36 hpf, the inner nuclear layer being produced between 36 and 48 hpf and the outer nuclear layer being produced between 48 and 60 hpf. Within each layer, neurogenesis takes place asynchronously and cells located in the ventronasal quadrant of the retina differentiate first and cells in the ventrotemporal region differentiate last^[1, 3, 4]. Neural progenitors remain multipotent until their final mitotic division and their fate largely depends on environmental signals^[4]. During their cell cycle, nuclei of progenitor cells migrate between the apical and basal surface of the neuroepithelium, with S-phase taking place at the basal surface and M-phase at the apical surface. Following cell division, newly born neurons migrate from the apical surface to their final location^[3, 4].

In teleosts, the postembryonic retina grows throughout life of the individual and new neurons continuously arise from two distinct populations of stem cells^[3]. One of these stem cell populations resides at the retinal periphery in an area termed the ciliary marginal zone. These stem cells remain multipotent and give rise to all retinal

lineages except the photoreceptor lineage. The second stem cell population resides in the inner nuclear layer and consists of slowly dividing Müller glia cells that give rise to rod and cone photoreceptors^[1-4].

2.2.2 The retinal pigment epithelium (RPE)

The RPE is a highly polarized epithelium with its apical surface facing the photoreceptor layer and its basal surface facing the external environment. Melanogenesis marks the onset of RPE differentiation at 24 hpf. The RPE is of immense importance for the correct patterning, function and structural maintenance of the neural retina. The mature RPE forms the outer blood retina barrier and tightly controls the neural environment via the selective transport of nutrients, solutes and metabolites between the choroidal vasculature and the subretinal space. Photoreceptor cells are most dependent on RPE function. First, the RPE protects retinal neurons from oxidative damage, which arises as a side effect of light absorption. Second, it recycles the visual pigment retinal and thereby maintains photoreceptor excitability. Third, RPE cells extend long cellular protrusions that interdigitate the outer segments of photoreceptor cells. This allows RPE cells to phagocytose potentially damaged tips of the outer segments, thereby maintaining photoreceptor integrity^[2, 5]. Not surprisingly plenty of the mutations that have been associated with photoreceptor cell dystrophies actually affect genes required for RPE function rather than for photoreceptor cell function^[1, 6].

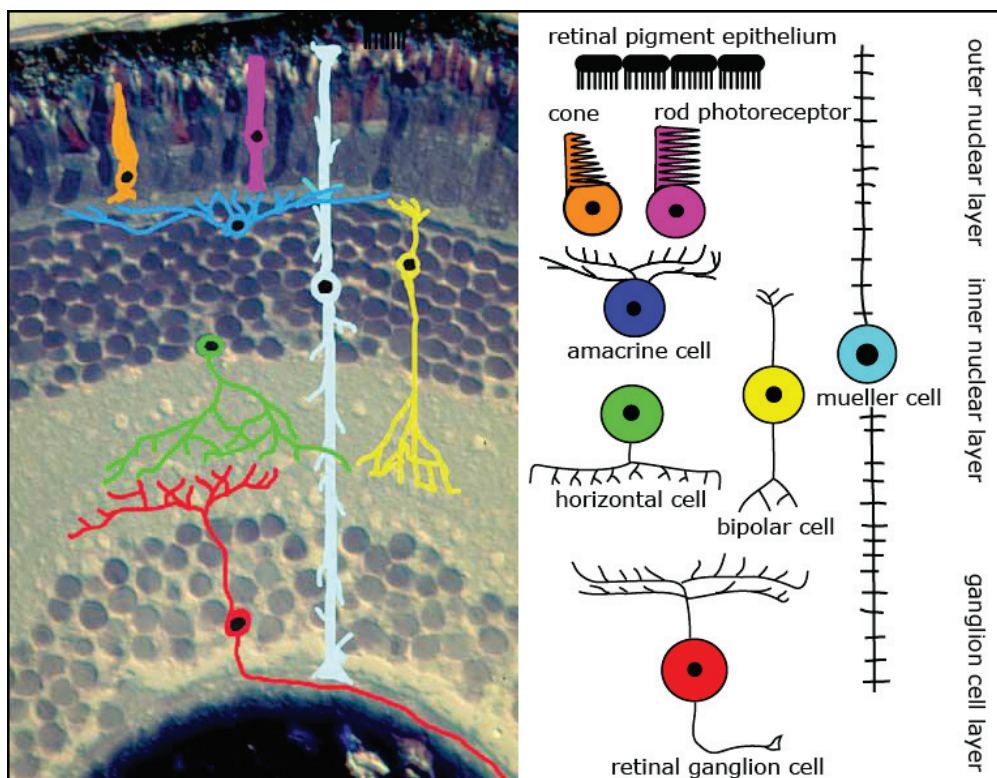


Figure 1: The major cell types in the adult zebrafish retina. Image source: www.pdn.cam.ac.uk

2.3 The cardiovascular system in zebrafish

The cardiovascular system maintains metabolic homeostasis by supplying tissues with nutrients and oxygen and removing waste products. It is the first functional organ system that develops during vertebrate embryogenesis, since general cell survival and function largely depends on blood supply^[7].

2.3.1 Development of the vascular tree

Blood vessels can form via two morphogenetic processes, vasculogenesis and angiogenesis. During vasculogenesis, individual angioblasts, or endothelial precursors, assemble into tubes, while further sprouting from those existing vessels occurs during angiogenesis^[7, 8].

Vascular development in zebrafish starts during early gastrulation, when angioblasts are specified in the ventral mesoderm. After gastrulation, individual angioblasts migrate towards the midline, coalesce and form the primary vessels via a vasculogenic process^[7]. The endoderm plays an essential role during vasculogenesis and is required for the correct timing of angioblast migration ^[7, 9]. It is therefore assumed that vasculogenesis only takes place in tissues containing endoderm, while tissues of mesodermal or ectodermal origin are primarily vascularized via angiogenesis ^[10, 11].

The molecular basis of primary vessel development appears diverse along the anterior-posterior body axis of the embryo since zebrafish mutants have been isolated that exhibit vascular defects only in distinct regions of the body ^[7, 12]. A variety of local extrinsic cues, some of which stem from the endoderm, specify angioblast behavior at different locations within the embryo^[7].

For a vessel to permit blood flow it needs to form an inner lumen. The dorsal aorta lumenizes via a cord hollowing process. Cells within the initial tube undergo junctional remodeling to develop apical-basal polarity. They secrete anti adhesive proteins on their apical side, leading to deadhesion of the cells apically and to the movement of cell-cell junctions to the basolateral side^[8]. The cardinal vein is formed by a different mechanism ^[7, 13]. Venous angioblasts sprout ventrally from the more dorsally located primordium in the trunk and coalesce around blood cells to form a tube^[13]. The primary circulatory loop is established by 22 hpf and the heart starts beating shortly after.

Most later developing vessels form by angiogenesis, growth and elaboration from these primary vessels. Angiogenesis is driven by external factors that promote both migratory behavior and cell proliferation in the so-called angiogenic sprout and guide the sprout towards their final location^[7]. Venous sprouts and arterial sprouts respond

to different signals. While VEGFA is required for arterial angiogenesis, it is dispensable for venous angiogenesis^[14].

Three mechanisms by which angiogenic sprouts can lumenize are known; cord hollowing, cell hollowing and budding. Cord hollowing proceeds similar to the previously described vasculogenic situation; endothelial cells lose apical-basal polarity to form the sprout and regain polarization during the cord hollowing process. Intersegmental vessels, which sprout dorsally from the dorsal aorta and cardinal vein, are formed by this mechanism. Other vessels, including brain vessels, form by budding, whereby apical-basal polarity is retained and the luminal space remains continuous with the parent vessel. Lumenization by cell hollowing requires a single cell layered sprout that lumenizes by the fusion of intracellular vacuoles. Whether this mechanism is indeed used during blood vessel development in zebrafish remains to be determined^[8].

2.3.2 Vascular development in the zebrafish eye

The development of the eye, like other tissues, requires the concomitant formation of a vascular system. In most vertebrates the neural retina is supplied by two independent vascular systems, the choroid and the inner retinal vasculature. The inner retinal vasculature is restricted to the inner part of the neural retina to not interfere with light absorption of the outer retinal layers. The choroidal vasculature, encompassing the retinal pigment epithelium, supplies the outer neural retina^[15].

The first intraocular vessels, termed hyaloid vessels, are thought to emerge from the mesodermal component of the POM surrounding the optic cup. POM cells migrate through the choroid fissure into the eye at approx. 18 hpf and assemble into the first intraocular blood vessels^[2]. By 2 dpf a network of vessels has developed around the medial side of the lens, which then expands towards the lens equator and merges into a single intraocular ring vessel. Concomitantly, a vessel system forms on the external surface of the developing eye. It includes three radial vessels and the inner optic circle, which surrounds the retina at the ciliary marginal zone^[16, 17].

The hyaloid vasculature surrounding the back of the lens is eventually replaced by the mature retinal vasculature that is associated with the retinal ganglion cell layer^[2, 16]. While in mammals the hyaloid vasculature regresses concomitantly with the development of the inner retinal vasculature, in zebrafish the hyaloid vessels are largely maintained in adults^[2]. At 15 dpf the hyaloid vessels lose contact with the lens and instead associate with the retinal ganglion cell layer to form the mature inner retinal vasculature^[16].

From 2.5 dpf the choroidal vasculature develops at the basal side of the RPE^[18]. As for the hyaloid vessels, it is believed that endothelial cells originate from the mesodermal component of the POM, while stromal cells, melanocytes and pericytes

are derived from the neural crest component. RPE derived signaling molecules are required for development of the choroidal vasculature^[15].

2.3.3 Structural differences between vessels

Dependent on their structure, function, size and permeability, blood vessels are subdivided into different classes. In general blood vessels consist of a polarized endothelium, which directly faces the blood stream with its apical side, and so-called mural cells, which support the endothelium on its basal side. The term mural cell generally refers to vascular smooth muscle cells and pericytes^[7, 8].

Functional and structural differences are found between arteries and veins and between large vessels and small vessels. Arteries transport blood from the heart to the periphery, while veins conduct it back to the heart. Arteries have to withstand high pressure and are therefore supported by a tight layer of smooth muscle cells and pericytes that stabilize the endothelium. In large vessels, neurons are embedded in the smooth muscle cell layer to regulate blood pressure. Veins do not have to withstand high pressure and are therefore associated with less mural cells than arteries. Veins contain venous valves, which develop from invaginations of the endothelial layer, to prevent back flow of the blood^[8, 14].

Blood vessel maturation occurs rather late during zebrafish development. While mural cells are found associated with the endothelium at 7 dpf, mature blood vessel walls only form by 1 month post fertilization^[19, 20].

The endothelium of large vessels does not contain fenestrations, is tightly packed due to the formation of tight junctions and does therefore prevent most fluid and nutrient exchange with the environment. Exchange is only possible at the interface between small arteries, called arterioles, and small veins, called venules formed by specialized structures, referred to as capillaries. The endothelium of capillaries is fenestrated and their tight junctions are loose, allowing quick diffusion of molecules. Capillaries are only supported by pericytes on their abluminal side, which play an essential role in permeability regulation and integrity maintenance^[19]. An exception is the CNS vasculature, where tight control of solute transport across the endothelium is necessary to maintain brain homeostasis and neuronal activity. Therefore the endothelium in the CNS lacks fenestrations and forms well structured tight junctions^[21, 22].

2.3.4 Regulation of endothelial permeability

Endothelial permeability primarily depends on the presence or absence of fenestrations and the strength of cell-cell contacts. Cell-cell adhesion can be regulated according to the acute needs of a tissue. During an inflammatory response for example the endothelium increases its permeability to facilitate extravasation of macrophages. Cell-cell contacts that regulate permeability are composed of adherens- and tight junctions^[23].

Adherens junctions

The most important adherens junction proteins expressed in endothelial cells are VE-cadherin and N-cadherin. They are targets for posttranslational modifications on their cytoplasmic tail, which control binding activity of adherens junctions to regulatory proteins. They are involved in various signaling pathways, most important the Wnt- and VEGF pathway. The Wnt effector β -catenin is usually bound to the cytoplasmic tail of cadherins and required to link adherens junctions to the actin cytoskeleton. Loss of β -catenin from junctional complexes has two effects. First, dissociation of cadherins from the cytoskeleton destabilizes cell-cell junctions and second, free β -catenin is able to translocate into the nucleus and activate the Wnt pathway^[23, 24]. VE-cadherins colocalize with VEGFR2 and counteract the proliferative effect while enhancing the survival effect of VEGF signaling^[23, 25, 26].

The importance of VE-cadherin in vascular permeability regulation was shown in vivo by blocking VE-cadherin expression in zebrafish embryos^[19, 27] and by injecting VE-cadherin antibodies into the mouse circulation^[23, 28]. VE-cadherin antibody administration in mice immediately increased vascular permeability in the lung and heart, but surprisingly the brain, muscles and skin were unaffected, arguing for different mechanisms regulating permeability in different tissues^[23, 28].

Tight junctions

The most important tight junction proteins found in the endothelium are claudin, occludin and JAM proteins. Intracellularly, tight junctions bind to zona occludin, which links junction proteins to the cytoskeleton and is therefore required for tight junction stability. Binding affinity of zona occludin to the actin cytoskeleton is determined by its phosphorylation state and Ca_2+ concentration. Zona occludin is involved in signaling pathways that regulate endothelial permeability, including Ras signaling^[23]. Endothelial and epithelial permeability is mainly determined by claudins. Claudins are either associated with the external layer of the cell membrane, the e-face, or with the internal layer of the cell membrane, the p-face, whereby associations with the e-face are more leaky than associations with the p-face^[23]. Claudin 5 is ubiquitously expressed in the endothelium. Interestingly, in the peripheral endothelium it is associated with the e-face, while in brain vessels it is associated with the p-face.

Claudin 3 expression is restricted to the brain endothelium and under normal circumstances is found on the p-face. However, in glioblastomas both claudin 3 and 5 are found to be associated with the e-face and in accordance glioblastomas lead to the formation of brain edema^[23, 29].

There are various mechanisms to regulate vascular permeability, many involving proteins that have not been discussed here. The intracellular assembly of proteins at tight- and adherens junctions includes numerous signaling molecules, which regulate permeability by either directly affecting the stability of junctional complexes or activating downstream targets^[23].

2.4 Barriers in the brain and retina

The microenvironment of the central nervous system and retina needs to be tightly controlled throughout life of the individual to ensure proper neuronal development and function. Ionic concentrations have to be kept within a narrow range, high amounts of glucose and amino acids have to be provided, potentially harmful substances have to be prevented from entering the brain interstitial fluid and metabolic waste products need to be removed. Barriers that control exchange of molecules between the brain interstitial fluid and blood are found on the level of the brain endothelium and on the level of the choroid plexus epithelium in the adult. Similar barriers are found in the retina. In mammals, but not in teleosts, a third barrier forms at the level of the arachnoid membrane^[30].

Endothelial and epithelial barriers are characterized by 5 elements.

1. **Tight junctions:** Tight junctions limit diffusion through paracellular spaces of a monolayer and thereby force molecules to take a transcellular route. The composition of tight junctions determines the properties of a barrier, such that some claudins are preferably found in leaky barriers and others in tight barriers. Loss of tight junctions leads to increased endothelial permeability, which might cause hemorrhaging, edema formation and loss of brain homeostasis.
2. **Limited transcytosis:** Transcytosis, which describes the uncontrolled vesicular transport of molecules through the cell, is limited in the brain endothelium and choroid plexus epithelium.
3. **Facilitated diffusion:** The brain and retina are highly metabolic tissues and require a high amount of nutrients and oxygen. Fast exchange of molecules across the monolayer is therefore necessary. Epithelial and endothelial barriers express numerous channels on their cell surface, which allow the passage of preferred solutes along a concentration gradient, a mechanism referred to as facilitated diffusion. Glucose transporters are most prominent.
4. **Active transport:** Since a lot of molecules need to be moved against a concentration gradient, active transport systems are necessary. An increased mitochondrial content is therefore characteristic for the brain endothelium. Some transport proteins establish electrochemical gradients that drive transport through co- and antiporters.
5. **Solute modification:** Brain barriers have the properties to either degrade solutes that should not enter the brain interstitial fluid (ISF) or modify them to substances that are useful for the neuronal tissue^[21, 31].

2.4.1 Neuroepithelial-ventricular barrier in the embryo

The first brain barrier that is established during embryonic development is the neuroepithelial - ventricular barrier, which is formed by neuroepithelial cells lining the inner lumen of the neural tube. The neural tube undergoes various morphogenetic processes to subdivide the neural tube into fore-, mid- and hindbrain, with the inner lumen forming the ventricular system^[32]. Unlike mammals, the zebrafish ventricular system is exposed to the dorsal surface of the embryo and the ventricles are only covered by a thin epithelium originating from the dorsal roof plate of the neural tube^[33]. The ventricles can therefore be easily observed in live zebrafish embryos.

The ventricles contain cerebrospinal fluid (CSF), which is produced by the neuroepithelium during early development. Initial ventricle expansion (from 18-22 hpf in zebrafish) requires integrity of the neuroepithelium^[34] and the activity of ion channels^[35]. Ion transport into the ventricular lumen is thought to generate an osmotic gradient over the neuroepithelial membrane, which causes fluid to inflate the ventricular space^[35]. Additionally, the neuroepithelium secretes proteoglycans, which contribute to passive fluid movement into the ventricles^[36]. While initial ventricle inflation only requires neuroepithelial function, further expansion depends on blood circulation. Zebrafish mutants displaying circulation defects, lack ventricle expansion after 22 hpf^[34].

The ventricular system plays an essential role during brain development. Intraluminal pressure exerted onto the neuroepithelium stimulates cell proliferation and developmental signaling molecules and neuroendocrine hormones in the embryonic CSF (eCSF) regulate development of the adjacent central nervous system^[37, 38]. The composition of eCSF changes during development and even differs between ventricles. Some eCSF components are not produced by the neuroepithelium. Rather they are produced by peripheral tissues, transported via the blood stream to the ventricular surface and moved through the neuroepithelial-ventricular barrier into the ventricular lumen^[39-41]. The cell layer that forms the neuroepithelial-ventricular barrier in the embryo is the precursor to the adult ependyma and I will term it "embryonic ependyma" for the remainder of this thesis.

2.4.2 The blood-CSF barrier in the adult

In the adult, cerebrospinal fluid production is restricted to the choroid plexus epithelium and in accordance with a different source its composition differs from eCSF. The choroid plexus epithelium is continuous with the ependymal epithelium lining the rest of the ventricular surface. While the choroid plexus epithelium forms a selective blood-CSF barrier, the ependymal epithelium in the adult is leaky, allowing fast exchange of molecules between the brain interstitial fluid (ISF) and the CSF^[42]. Uniformly beating cilia located on ependymal cells maintain CSF movement through

the ventricular system^[43]. The choroid plexus consists of a microcapillary network surrounded by stroma and epithelial folds extending into the ventricular space. Although the endothelium forming the blood-brain barrier lacks fenestrations, the capillary network within the choroid plexus is fenestrated. Diffusion and transport into the CSF is only controlled at the level of the choroid plexus epithelium^[42].

In zebrafish, choroid plexus epithelial progenitors become specified by 36hpf and form a continuous epithelium in the hindbrain and forebrain ventricles by 3 dpf. By 6 dpf the hindbrain choroid plexus displays the characteristic morphology found in mammals, consisting of a microcapillary network and epithelial folds. It remains to be determined, when the choroid plexus becomes functional and takes over CSF production^[44].

2.4.3 Blood-brain barrier (BBB)

Initially the neural tissue is vascularized by a fenestrated and leaky endothelium. The endothelium develops its barrier properties only after interaction with the local neural tissue^[30]. In zebrafish embryos, blood-brain barrier maturation starts at 2.5 dpf^[45].

Various cell types are involved in the development, maintenance and regulation of the BBB, most important are astrocytes and pericytes. Loss or dysfunction of either of these cell types severely affects endothelial integrity and neural homeostasis^[21, 46].

The number of pericytes embedded in the basal lamina of the endothelium is strongly increased in the brain compared to the periphery. They secrete factors that promote tight junction formation in endothelial cells. For example, pericyte derived angiopoietin induces occludin expression in brain endothelial cells^[47]. Under hypoxic conditions pericytes dissociate from the endothelium thereby increasing endothelial permeability^[48].

Astrocytic endfeet are continuous with the endothelial basal lamina and this interaction is essential for the induction and maintenance of blood-brain barrier characteristics. Astrocytes mainly communicate with the endothelium via gap junctions. Ca₂⁺ signaling seems to be the primary pathway to regulate endothelial permeability by astrocytes. The perivascular astrocytic endfeet show a high density of so-called orthogonal arrays of particles (OAPs), containing K⁺ channels and water channels. Astrocytes buffer K⁺ concentrations in the interstitial fluid after neuronal exercise and remove water produced by glucose metabolism. They take up K⁺ and water at a distant site and deposit it in the perivascular space. Moreover, they directly sense neuronal activity and in association with blood vessels they regulate transport across the endothelium according to neuronal needs^[46].

The extracellular matrix is also an essential component of the blood brain barrier and its disruption is associated with increased permeability. It consists among others of various laminin subtypes, collagens, heparan sulphate proteoglycans, osteonectin,

fibulin1 and 2 and thrombospondin 1 and 2. Various ECM receptors, most importantly integrins, are expressed in astrocytes, endothelial cells and pericytes, and anchor the cells to the extracellular matrix^[49]. Collagen 4a and integrin α_v mutations in mice lead to intracerebral hemorrhage of microvessels and highlight the importance of cell- ECM interactions in cerebral vessel integrity^[50, 51].

2.4.4 Blood-retina barrier (BRB)

In the neural retina, the blood-brain barrier is divided into two regions, the inner and outer blood-retina barrier. The inner blood-retina barrier is found at the level of intraretinal blood vessels and corresponds to the endothelial portion of the blood brain barrier. As in the brain, adjacent glia cells induce barrier properties in the retina. The outer BRB closely resembles the ventricular portion of the BBB. It is formed by the retinal pigment epithelium, which is, like the ventricular epithelium, of neuroepithelial origin^[31]. The RPE is a polarized epithelium facing the outer photoreceptor layer with its apical side and the choroidal vasculature with its basal side. The RPE transports ions, water and metabolites from the subretinal space to the choroidal vasculature and delivers nutrients, glucose and fatty acids from the blood to the neural retina. It tightly controls ion composition of the subretinal space to maintain neuronal excitability^[5, 6].

A recent study showed that in zebrafish the retinal vasculature develops barrier properties at 3 dpf and is only then able to restrict diffusion of low molecular weight molecules^[45].

2.5 Aims of this work

This study aims to investigate the cellular mechanisms underlying retinal degeneration in the zebrafish mutant "*modern art*" by

1. performing general phenotypical analysis;
2. determining whether the eye phenotype is caused by cell-intrinsic or cell-extrinsic mechanisms (cell transplantation experiments);
3. investigating whether vascular abnormalities contribute to retinal degeneration;
4. identifying the mutant locus.

3. Results

3.1 The *modern art* mutant displays degeneration of various tissues, including the brain and retina.

The *modern art* (*moda*) mutant was selected from an ENU mutagenesis screen due to its degeneration in the dorsal retina. Specifically, retinal pigment epithelium (RPE) cells are lost from the dorsal side of the eye at around 2.5 dpf (days post fertilization) and appear to move as clusters towards the anterior head region (Fig. 2j). Until 2 dpf mutants are indistinguishable from their siblings and exhibit no apparent developmental defects (Fig. 2a,b). Tissue degeneration sets in at 2 dpf, beginning with the fins (Fig. 2i,j) and followed by the vasculature (Fig. 2m,n), the dorsal anterior retina (Fig. 2i,j) and the dorsal anterior brain (Fig. 2k,l). The jaws are either absent or reduced (Fig. 2k,l), pigments lose their defined line-shaped morphology on the tail (Fig. 2m,n) and the otic vesicle collapses (Fig. 2k,l). Mutant embryos die between 3.5 and 4 dpf.

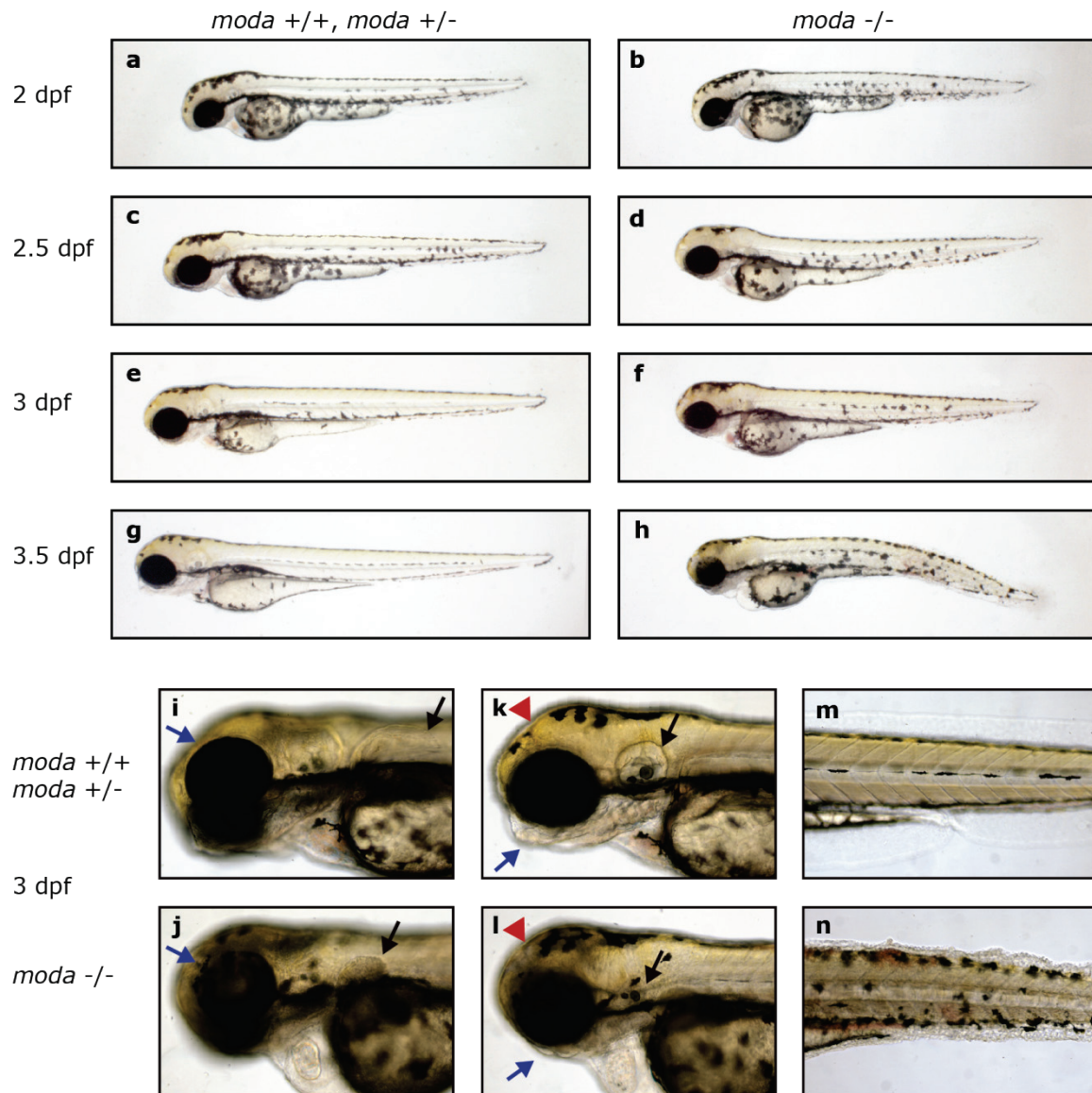


Figure 2: Live images of the *modern art* mutant between 2 and 3.5 dpf. (**a-n**) Live images of *moda* mutants and siblings pictured at the stage indicated on the left, (**i-j**) retina (blue arrow) and fin (black arrows) phenotype, (**k-l**) jaw (blue arrow), otic vesicle (black arrow) and brain (red arrowhead) phenotype, (**m-n**) tail pigmentation and hemorrhaging.

3.2 Early eye development is not affected in *moda* mutants, but the dorsal retina starts to degenerate at 2 dpf

As I was specifically interested in the eye phenotype, I crossed *moda* carriers to the *tg(ath5:GFP)* transgenic line, labeling the retinal ganglion cell (RGC) layer. RGC neurogenesis is not affected in *moda* mutants and retinal ganglion cell axons connect to the contralateral tectum (Fig. 3a-d). The optic nerve (Fig. 3c,d) and tectum (Fig. 3a,b) are smaller in mutants and one does not observe an *ath5:GFP* signal from the olfactory bulbs (Fig. 3a,b). At 3 dpf the dorsal anterior part of the retinal ganglion cell layer becomes disorganized and *ath5:GFP* positive cells spread all over the retinal layers (Fig. 3e,f).

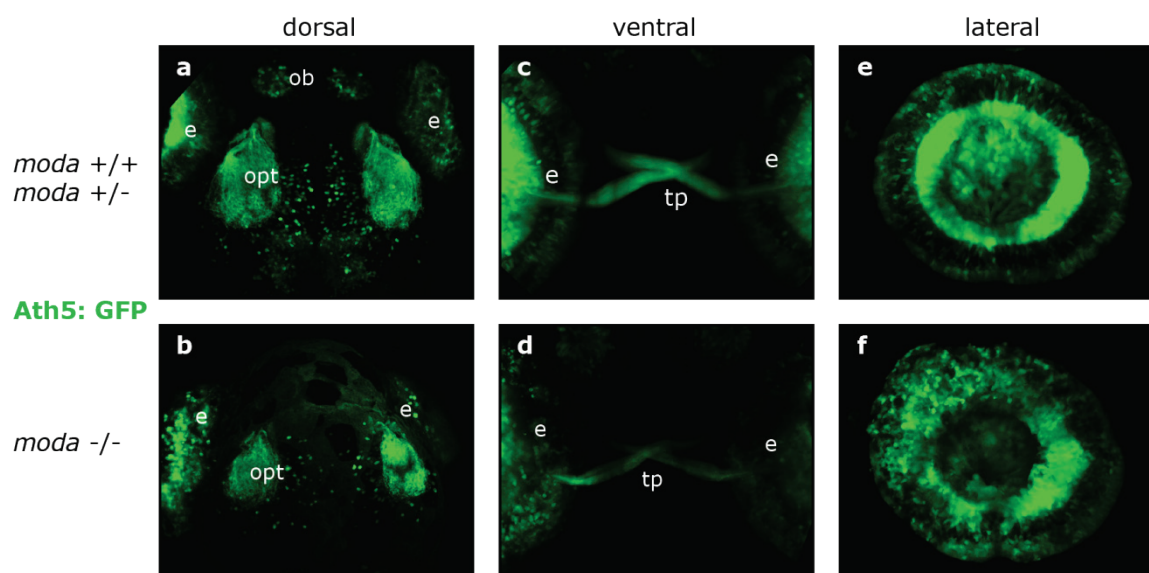


Figure 3: Dorsally located retinal ganglion cells become distributed all over the retinal layers. *ath5-GFP* transgene expression in live *moda* mutants at 3 dpf. (a,b) dorsal view, anterior up, (c,d) ventral view, anterior up, (e, f) lateral view, anterior to the left. ob: olfactory bulbs, opt: optic tectum, e: eye, tp: tectal projections

To investigate the retina phenotype in more detail, I performed histological sections, which I stained with toluidine blue (Fig. 4, 5). In sections the phenotype could be first detected at 2 dpf by the absence of RPE cells from the dorsal anterior RPE and the presence of occasional clusters of RPE cells inside the dorsal retina (Fig. 4). The neural retina is not affected at this stage (Fig.4, Supplementary Fig. 1d-f).

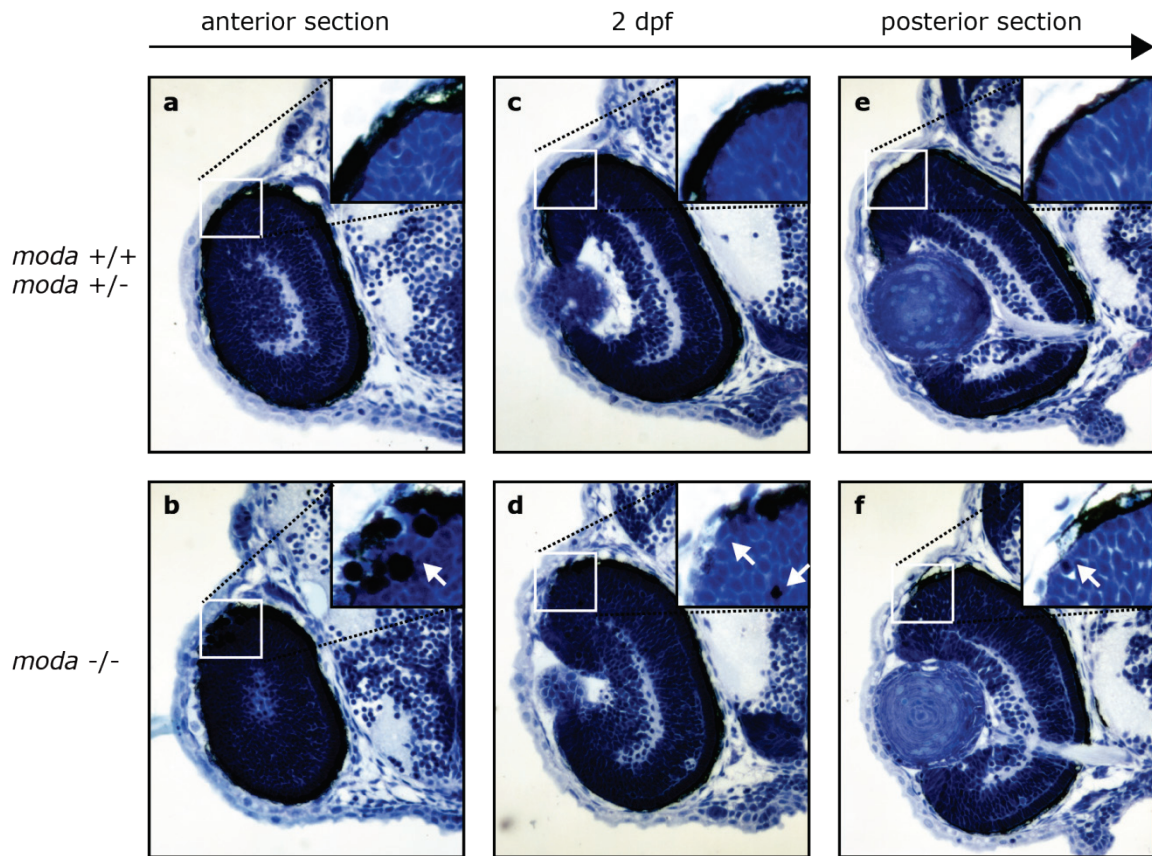


Figure 4: The dorsal anterior RPE layer becomes disorganized at 2 dpf. Serial coronal sections of the eye at 2 dpf stained with toluidine blue. Inserts magnify regions of RPE loss and displacement into the retina (white arrows).

At 3 dpf there is some variability in extent the eyes are affected in mutants. In weakly affected mutants the retinal layers are generally intact in the ventral eye and are only disrupted dorso-anteriorly (Fig.5d-f). In severely affected mutants the whole retina is disorganized (Fig. 5g-i). The dorsal anterior part of the retina stretches and retinal cells move in between the brain tissue and the skin epithelium (Fig. 5g, Supplementary Fig. 1g-i). RPE cells are not stretched as uniformly as the neural retina and rather appear in clusters (Supplementary Fig. 1g). In all mutant embryos that have been sectioned I detect some small, round, intensely staining particles between the lens and the RGC layer, in severely affected regions also between the lens and the skin epithelium and in regions of RPE degeneration in the photoreceptor layer. These particles have been described as apoptotic cell corpses^[52, 53] (Fig. 5d-i, Supplementary Fig. 1g-i). The mutant retina is severely underdeveloped compared to siblings.

In summary, early eye development is not affected in *moda* mutants. The eye stops developing at 2.5 dpf and degeneration sets in at the dorsal anterior part of the RPE.

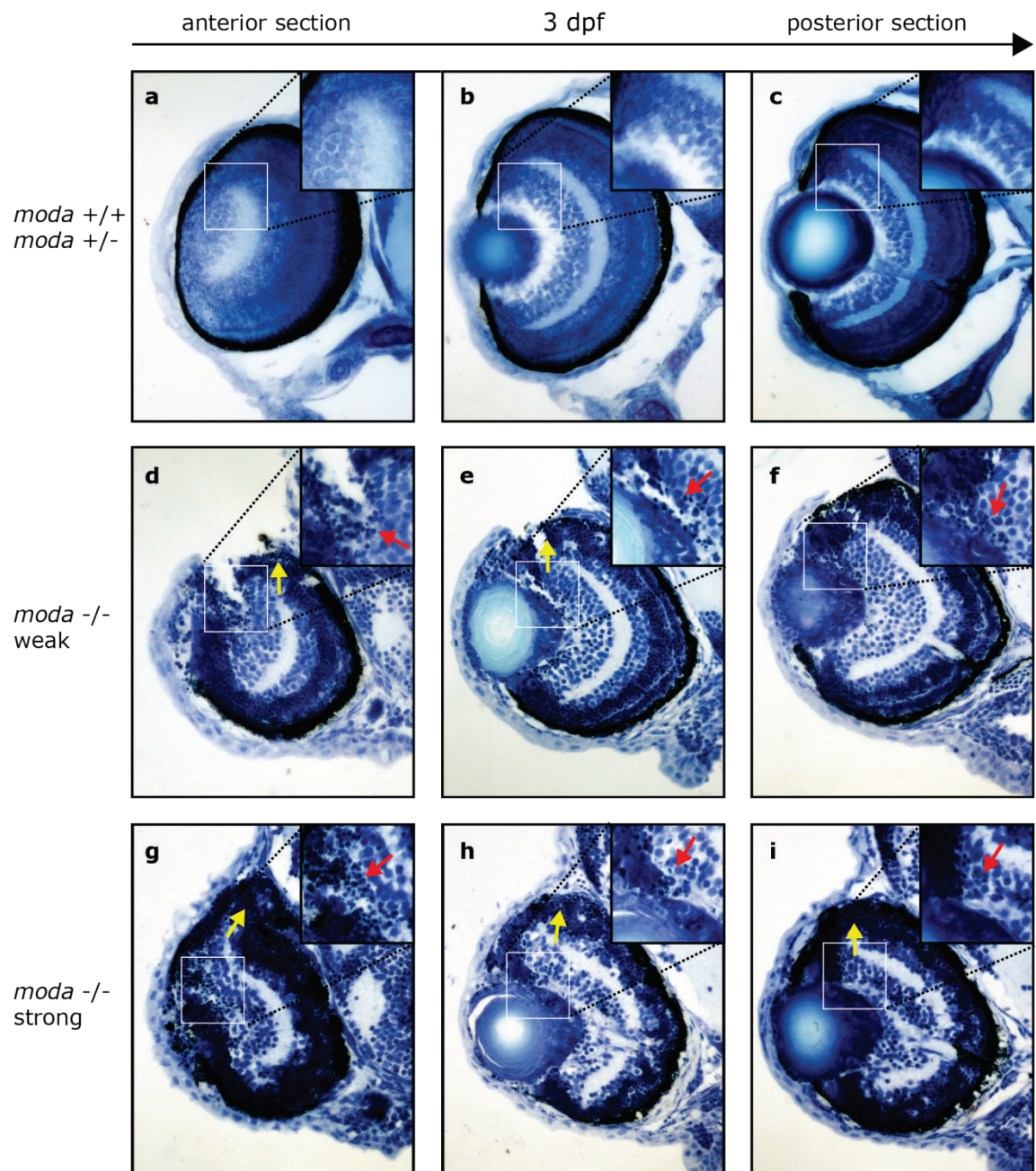


Figure 5: Retinal organization is disrupted in 3 dpf *moda* embryos. Serial coronal sections of the eye stained with toluidine blue. Inserts magnify regions, where apoptotic cell corpses are detected (red arrows). Yellow arrows indicate RPE loss from the dorsal anterior retina

3.3 Actively migrating retinal pigment epithelium cell clusters co-localize with the macrophage specific marker L-plastin

To investigate more closely how RPE cell clusters become ectopically located outside and inside the retina, one mutant eye was imaged over 24 hours with the onset of RPE degeneration (Fig. 6, Supplementary Video).

The time-lapse movie revealed two kinds of movements in the dorsal retina underlying the displacement of clustered retinal pigments. At the beginning of the movie (2.4 dpf), when the brain tissue is still healthy, pigments move forwards and backwards towards the anterior head region, sometimes appearing to move with the blood flow (Fig. 6a-e, yellow arrow in Fig. 6a-c tracks a pigment looping in the blood vessels). After 12 hours of imaging (3 dpf) the individual movement of pigmented structures ceases. Instead they move synchronously towards the anterior head region due to a stretching of the entire retina (Fig. 6g-i). The white arrow in Fig. 6i shows a large fragment of the RPE getting disconnected from the eye by stretching. Until 2.8 dpf (Fig. 6a-f) structures from the vasculature can be clearly observed on the brain surface and dorsally to the eye. Later these structures are lost, indicating a high rate of apoptosis (Fig. 6g-i).

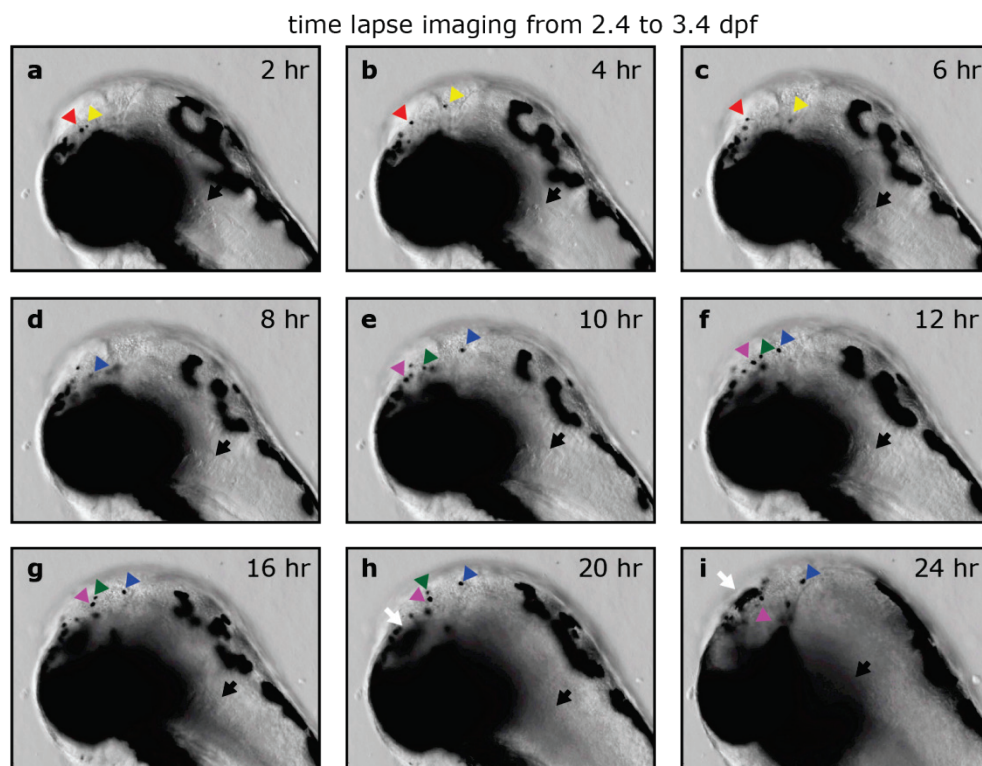


Figure 6: RPE cell clusters move away from the retina. Timelapse images of a mutant eye between 2.4 and 3.4 dpf, (a-f) micrographs taken in 2hr intervals, (f-i) micrographs taken in 4 hr intervals. The black arrowhead indicates vasculature structures, which are lost at 3 dpf (h,i). The white arrow in i indicates a big part of the RPE that gets disconnected by stretching. Differently colored arrowheads track individual pigmented clusters.

A simple explanation for pigments moving away from the eye would be that dead retinal pigment epithelium cells are taken up by macrophages.

In order to test this possibility I investigated whether individual pigmented clusters co-localize with the macrophage specific marker, L-plastin (Fig. 7).

Since the retinal ganglion cell layer stretches to the same extent as the RPE cell layer, I used the *ath5*-GFP transgene to distinguish between RPE cell clusters that have been displaced by active movement and RPE cell clusters that have been displaced by stretching. Pigmented structures residing in the vicinity of *ath5*:GFP positive cells were not expected to co-localize with a macrophage.

In 8 embryos all pigmented structures that were not in the vicinity of *ath5*:GFP positive cells co-localized with the macrophage marker (Fig. 7c,d). In 2 embryos, however, none of these pigmented structures co-localized with the macrophage marker (Fig. 7a). Importantly, while macrophages can be detected at the back of the eye in these embryos (Fig. 7b), the area surrounding these non-co-localizing pigments is depleted from macrophages (Fig. 7a). This may suggest that macrophages have taken up RPE cells, transported them away but have undergone cell death due to toxic effects in this highly apoptotic area.

Roundish shaped pigments were also found in the tail and often co-localize with the macrophage marker (Fig. 7e,f).

In general, these results strongly suggest that RPE cell clusters are not moving independently. Rather apoptotic/necrotic RPE cells are carried away by macrophages.

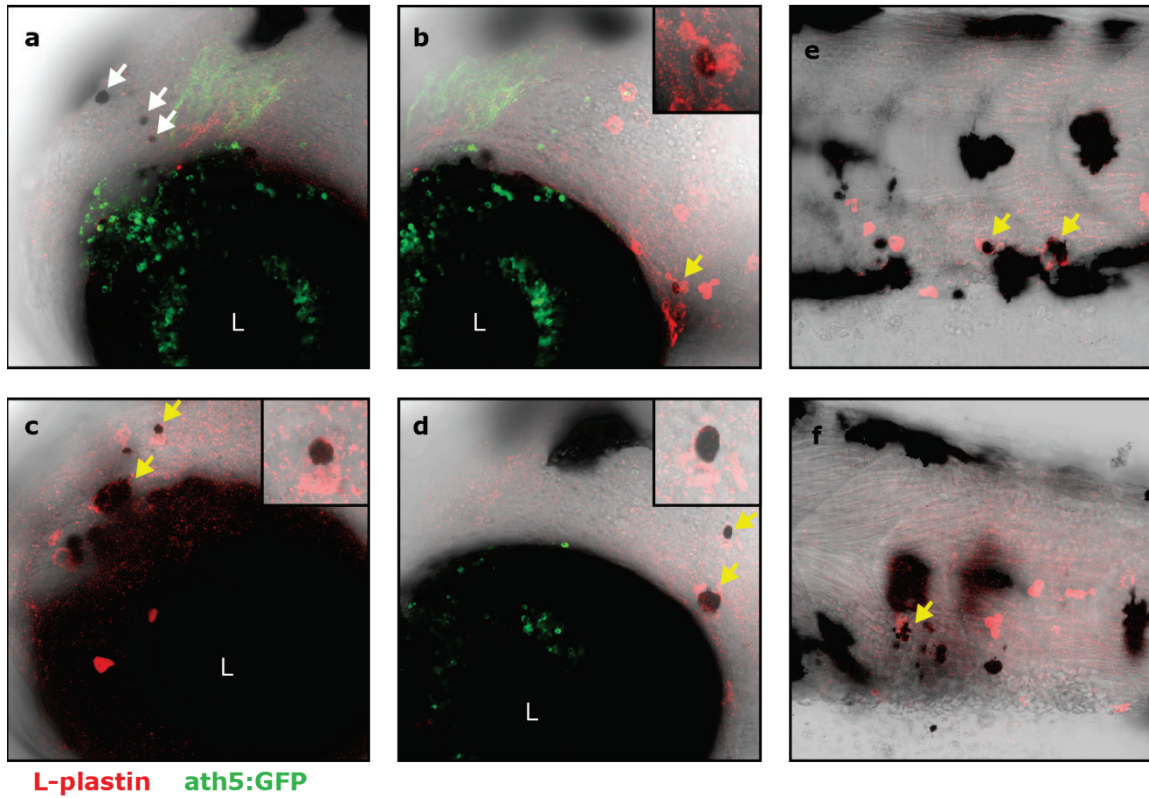


Figure 7: Displaced RPE cell clusters co-localize with the macrophage specific marker L-plastin. Antibody staining for L-plastin shown in red, *ath5:GFP* transgene expression shown in green. **(a,b)** anterior eye (a) and posterior eye (b) of the same *moda*^{-/-} embryo; **(c, d)** eye of 2 *moda*^{-/-} embryos, **(e,f)** tail of 2 *moda*^{-/-} embryos. inserts show magnification of pigment/macrophage co-localization, yellow arrows indicate pigment/macrophage colocalization, white arrows indicate missing colocalization, L: lens

3.4 The *moda* mutation causes extensive apoptosis in the brain, eye, tail and fins

In order to determine the sites of apoptosis in *moda* mutants, I stained embryos at different stages by Terminal deoxynucleotidyl transferase dUTP nick end labeling (TUNEL) (Fig. 8). At 2 dpf apoptosis can be first detected in a few embryos and is found in the vicinity of the brain ventricles, including the embryonic ependyma, and the very tips of the pectoral fins (Fig. 8b). At 2.5 dpf additional apoptotic regions are found in the external layers of the retina and in the tail (Fig. 8d). At 3 dpf the brain and retina are extensively affected by cell death, whereby degeneration is most severe in the dorsal anterior area of both tissues (Fig. 8f).

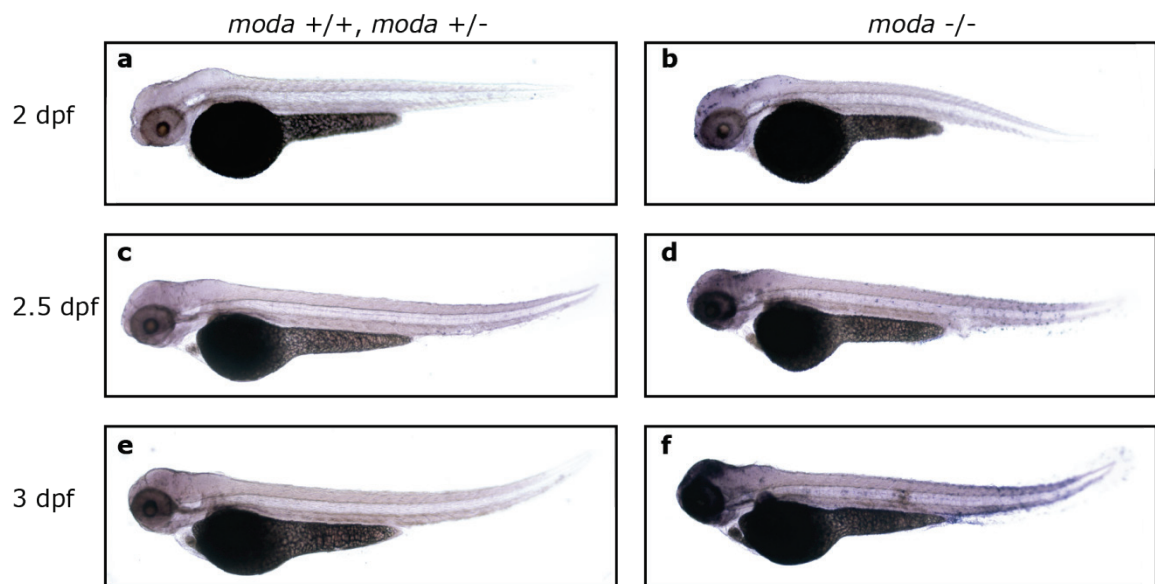


Figure 8: Apoptosis affects the ventricles, the dorsal anterior retina and brain, the fins and the tail. TUNEL staining of embryos at the stage indicated on the left.

In order to test if all the observed *moda* phenotypes are a result of cell death, I tried to rescue apoptosis by p53MO injection and Caspase Inhibitor treatment, which are commonly used methods to rescue apoptosis in zebrafish^[54, 55]. However, in *moda* mutants I failed to rescue apoptosis in every tissue under both conditions (Supplementary Fig. 2).

Thus, cell death is either driven by a programmed, caspase-independent mechanism or the standard concentrations of p53MO and Caspase Inhibitor are too low to rescue apoptosis in *moda* mutants.

3.5 Extensive cell death in *moda* mutants is not caused by oxidative damage

The only caspase-independent programmed cell death pathway described so far is exclusively activated by external factors causing severe cellular damage, including reactive oxygen species^[56]. In order to test if *moda* mutants suffer from increased oxidative damage, I measured endogenous β -galactosidase activity, which becomes elevated in response to oxidative stress^[57]. No significant difference in β -galactosidase activity could be detected in 3 dpf embryos (Fig. 9), indicating that apoptosis in *moda* mutants is not caused by oxidative damage.

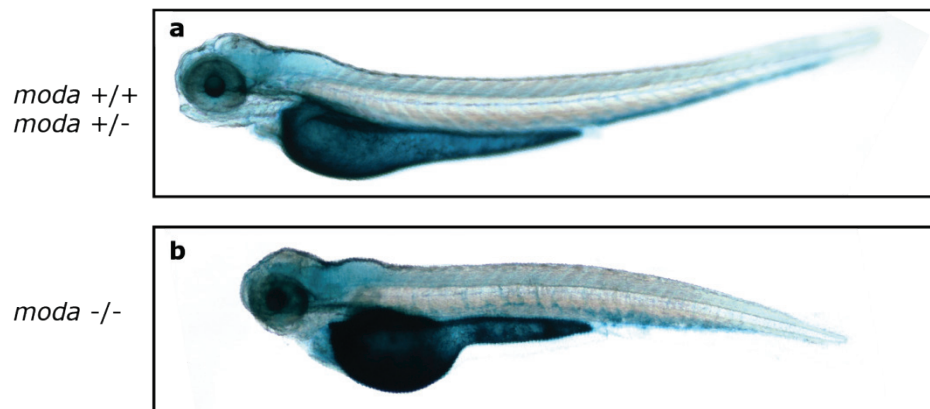


Figure 9: β -galactosidase activity is not elevated in 3 dpf *moda* mutants. X-gal staining

3.6 Cell death and disruption of retinal organization is caused by a non-cell autonomous mechanism

To analyze whether the *moda* phenotype is caused by a cell-intrinsic or cell-extrinsic mechanism, I performed transplantation experiments.

Given that RGCs become displaced in 3 dpf *moda* embryos, I transplanted *ath5:GFP* positive cells from *moda* mutants and siblings into wildtype embryos (Fig. 10a,b). Mutant retinal ganglion cells properly integrate into the RGC layer in a wildtype environment and do not appear in the wrong layer at least until 4 dpf. The mosaic eye is morphologically indistinguishable from a wildtype eye.

In order to investigate the general survival of *moda* cells in a wildtype environment, I randomly transplanted mutant cells, labeled with *H2B:RFP* mRNA, into a wildtype embryo (Fig. 10c-f). Mutant cells can still be detected in a wildtype embryo at 4 dpf in various tissues. I could even observe mutant cells in the dorsal forebrain and in the vicinity of the hindbrain ventricle, tissues that are highly apoptotic in 3 dpf *moda* mutants.

These results argue for cell extrinsic factors causing disruption of the dorsal RGC layer and extensive cell death in *moda* mutants.

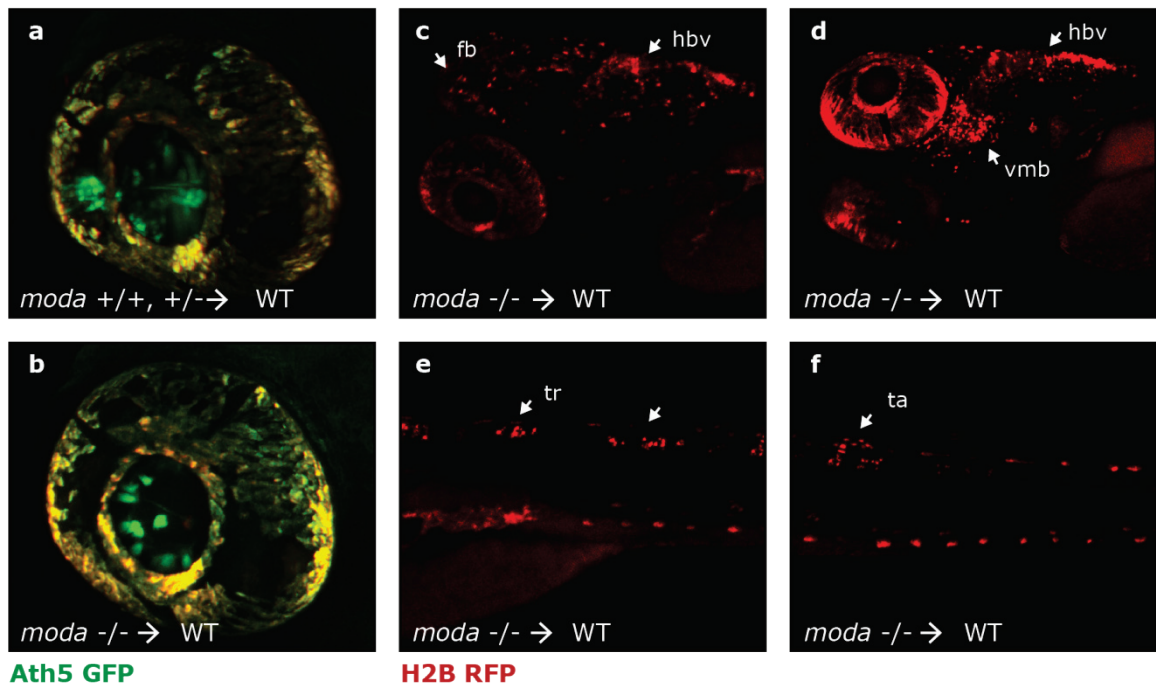


Figure 10: Mutant cells transplanted into a wildtype embryo properly integrate to form various tissues. Pictures taken at 4 dpf. (a,b) *ath5:GFP* positive *moda*^{-/-} (b) and sibling (a) transplants in a WT eye, (c-f) *moda*^{-/-} (*H2B:RFP*) transplant in a WT head (c,d), trunk (e) and tail (f). (c) dorso-lateral view, (d) ventro-lateral view, (e,f) lateral view
fb: forebrain, hbv: hindbrain ventricle, vmb:ventral midbrain, tr: trunk, ta: tail

3.7 The brain stops developing at 2 dpf and shows morphological defects in the embryonic ependyma

Since the brain is most affected by cell death, I investigated the general brain morphology in *moda* mutants (Fig. 11, Supplementary Fig. 3-5). Antibody staining for acetylated tubulin and sv2 and cross sections of the brain revealed no apparent differences between mutant and sibling at 2 dpf (Fig. 11 a-d). The mutant's optic tectum is slightly smaller (Fig. 11a,b) and ventricle fusion has not progressed as in its sibling (Fig. 11c,d). This may be due to a slight difference in age between this mutant and its respective sibling or indicate a developmental delay in *moda* already at this stage. Like the eye and possibly the whole embryo, the brain does not continue to develop after 2 dpf (Fig. 11e,f). Moreover, in severely affected mutants cells lining the ventricular surface adopted a bubble-like morphology and have about 20 times the size than under physiological conditions. I also observe this kind of cell morphology in the epithelium behind the eye that may correspond to the pia mater (Fig. 11f arrows). In summary, the mutant brain stops developing around 2 dpf and shows morphological defects at the ventricular surface after 3 dpf.

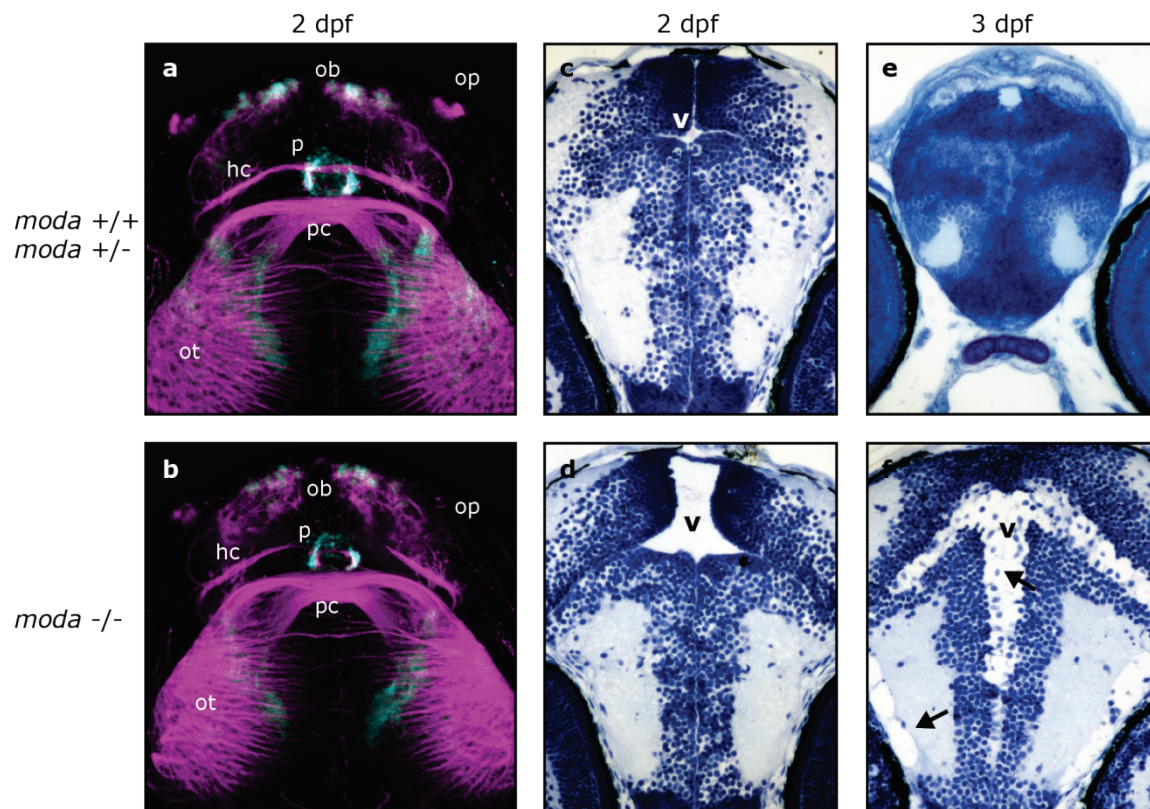


Figure 11: The *moda* brain stops developing at 2 dpf and shows morphological defects at the level of the ventricles. (a,b) Antibody staining for acetylated tubulin (magenta) and sv2 (blue) in 2 dpf *moda* embryos, (c,d) coronal sections of the midbrain at 2 dpf, (e,f) coronal sections of the midbrain at 3 dpf. ob: olfactory bulbs, op: olfactory pit, p: pineal, hc: habenular commissure, pc: posterior commissure, ot: optic tectum

3.8 Cell death in the brain and retina is rescued by a loss of blood flow

Given that the *moda* phenotype seems to be triggered by external and systemic stimuli, I decided to focus on the vasculature. When observing *moda* embryos under the light microscope one can first detect vascular defects at 2.5 dpf. The blood flow slows down despite normal heart beat frequency and cell/protein aggregates appear in the circulation. At 3 dpf blood flow is obstructed in parts of the brain and the tip of the tail. In addition, hemorrhaging is observed in various tissues, behind the eye, inside the ventricles, in the brain and tail (data not shown). Fluid accumulates in and surrounding the anterior brain, leading to detachment of the skin epithelium from the dorsal anterior brain tissue (Fig. 13b, blue arrow).

Since hemorrhaging and fluid accumulation may cause extensive cell death independent of Caspase activation, I wanted to investigate the *moda* phenotype in the absence of blood flow. I therefore crossed *moda* carriers to *bloated* (*blo*) carriers, which harbor a mutation that abolishes blood flow in homozygous mutants. The *bloated* mutant was identified in the same ENU mutagenesis screen as the *moda* mutant.

Blo mutants are completely immotile, their yolk is thickened and they do not grow to the same extent as their siblings. They have a weakly beating heart with unusual morphology. When injecting fluorescein into either heart chamber the dye does not leave the chamber into which it was injected, demonstrating complete lack of circulation (Fig. 12a-d). The endothelium forms properly (Fig. 12e-l). As is typical for a vasculature mutant the ventricles are small, as they never fully expand in the absence of blood flow (Fig. 12g,h)^[34]. *Blo* mutants develop a huge edema in the pericardium and from 4 dpf onwards also behind the eye. About 30% do not develop the otic vesicle properly, displaying three instead of two otholites (data not shown). Immotility in combination with a weakly beating heart suggests a general muscle defect underlying the *blo* phenotype. *blo* mutants die at 6 dpf.

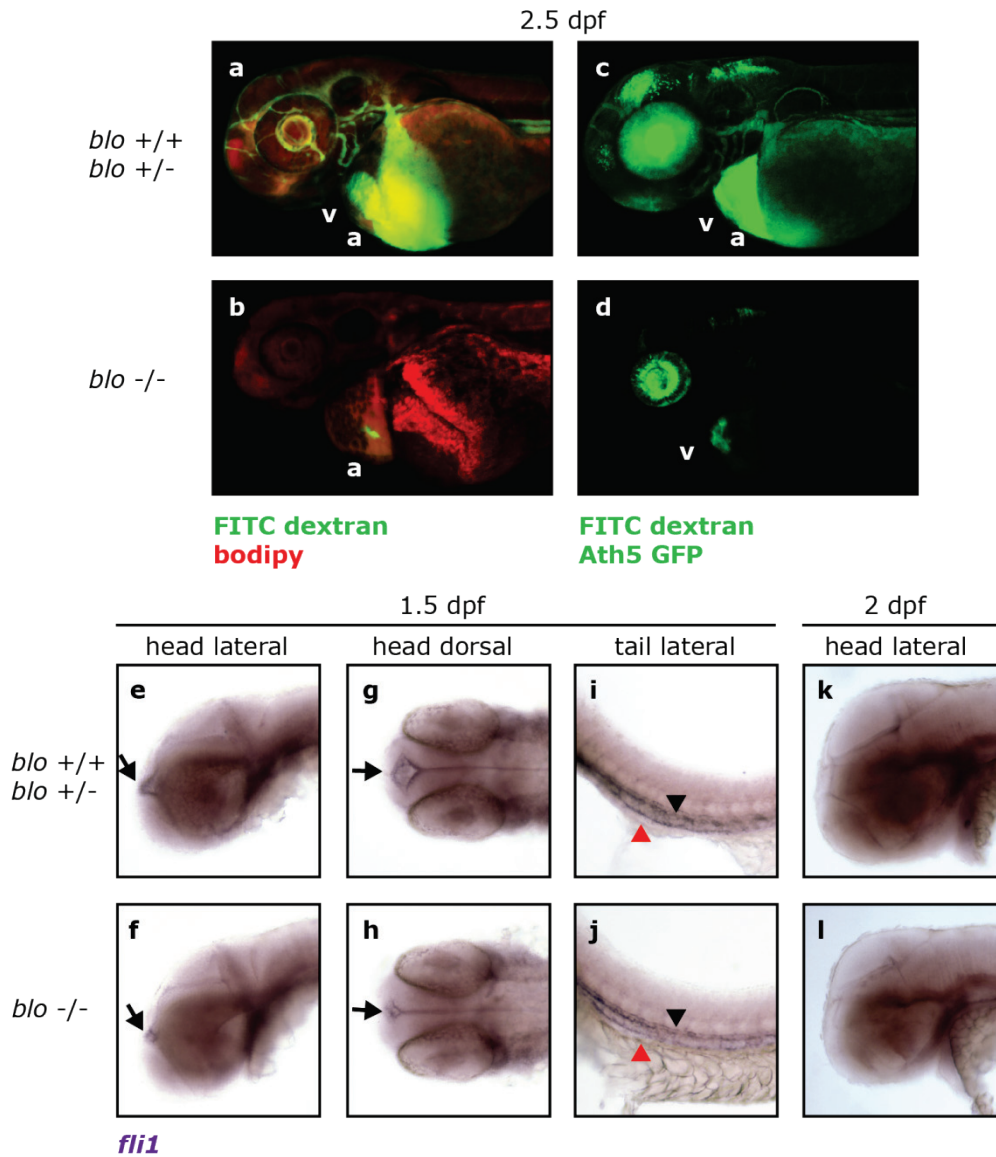


Figure 12: *blo* mutants lack circulation without showing endothelial defects.

(a-d) Microangiographie of 2.5 dpf *blo* embryos, (a,b) fluorescein was injected into atrium, (c,d) fluorescein was injected into ventricle, (e-l) in situ hybridization of *fli1* labeling the endothelium. Arrows in e-h indicate the forebrain ventricle, black and red arrowheads in i,j indicate the dorsal aorta and the cardinal vein, respectively.

From the *blo* x *moda* cross I obtained carriers of both mutations, allowing me to investigate the contribution of blood flow to the manifestation of the *moda* phenotype. At 2 dpf, fin degeneration can be observed in both *moda* and *blo/moda* double mutants (Fig. 13e-h, Supplementary Fig. 7a-l). At 2.5 dpf, siblings and *blo* single mutants start to develop the jaws, which are reduced or absent in *moda* and *blo/moda* double mutants (Fig. 13i-l, Supplementary Fig. 8). Vascular defects can be first observed in *moda* mutants and pigments change their shape mainly at sites of hemorrhaging. Pigmentation is not affected in *blo/moda* double mutants (Fig. 13m-p, Supplementary Fig. 7m-x). At 3 dpf extensive apoptosis is observed in *moda* mutants, especially in the dorsal anterior brain, retina and tectum, along the ventricular surface, in the tail and fins (Fig. 13v). The RPE layer and the neural retina degenerate, leading to displacement of dorsally located RPE cell clusters (Fig. 13f) and disorganization of the dorsal anterior retinal ganglion cell layer (Fig. 13r). Cell death is not observed in the brain, retina and tail of *blo/moda* double mutants (Fig. 13x) and overall eye morphology, according to DIC microscopy and *ath5:GFP* expression, seems completely unaffected (Fig. 13 h and t, respectively). Apoptosis in the fins is however comparable to *moda* mutants (Fig. 13h,x). In *moda* mutants the otic vesicle collapses at 3 dpf. At this stage the otic vesicle is still properly inflated in *blo/moda* double mutants (Fig. 13l, Supplementary Fig. 8a-h), however it appears collapsed at 4.5 dpf (data not shown).

94% of *moda* single mutants do not survive until 4 dpf. *blo/moda* double mutants are still alive, but apoptosis can be observed in the central nervous system (data not shown) and lateral parts of the pericardial edema appear to have burst (Fig. 13d, black arrow). *blo/moda* double mutants die between 4.5 and 5 dpf, approximately 14 hours later than *moda* single mutants.

From these results one can conclude that the eye phenotype, the pigmentation defect and extensive apoptosis in the brain and tail are caused by a blood flow dependent mechanism. In contrast, early *moda* phenotypes, including fin degeneration and jaw defects, cannot be rescued by depletion of blood flow. Importantly, early death of *moda* mutants cannot be entirely attributed to the vasculature, since *blo/moda* double mutants die only half a day later than *moda* mutants, but still 1.5 days earlier than *blo* mutants.

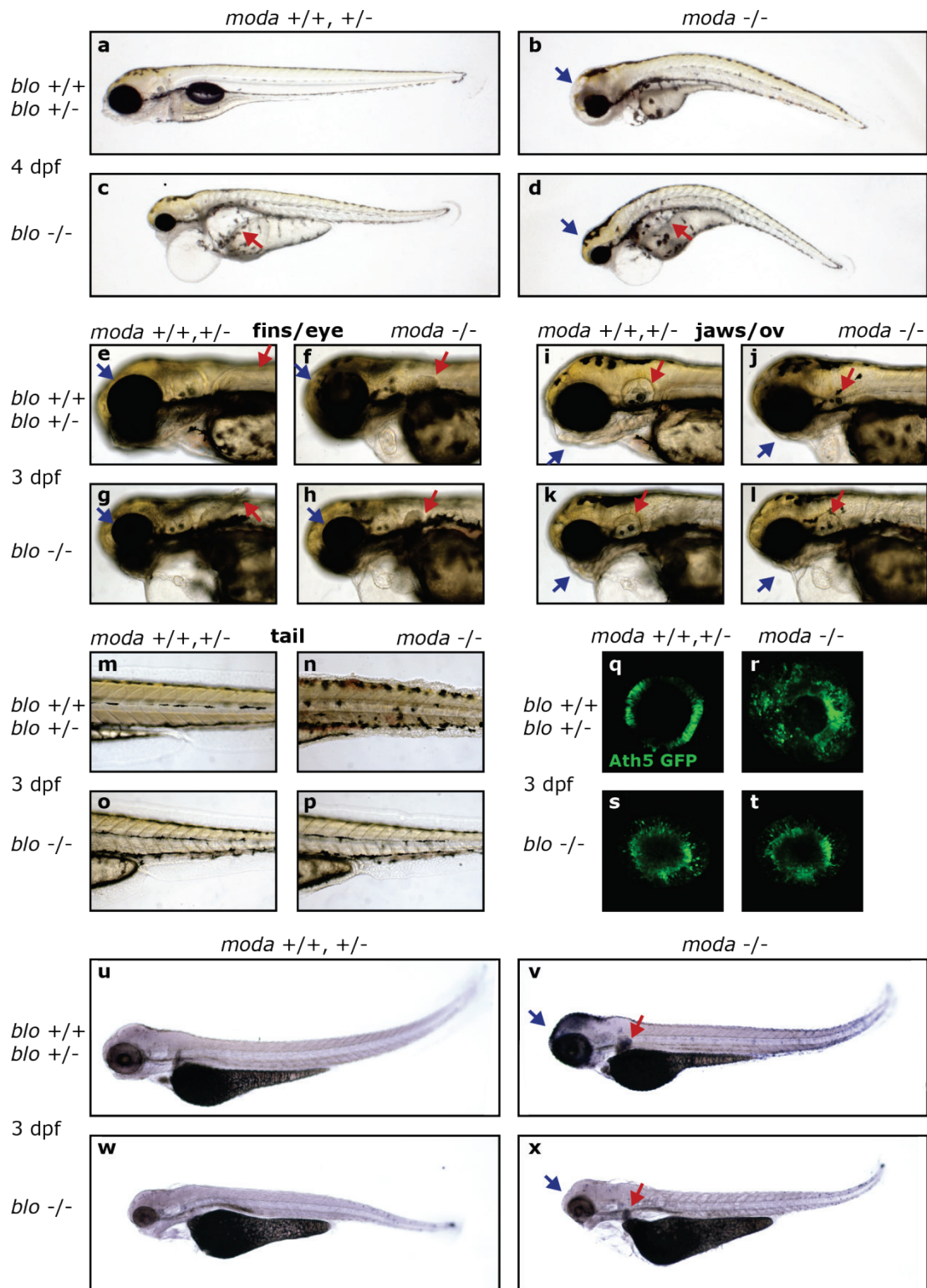


Figure 13: Retinal and CNS degeneration is rescued by a loss of blood flow. **(a-d)** Live images of *blo/moda* embryos at 4 dpf. Blue arrow indicates brain degeneration, which is rescued in *blo/moda*, red arrow indicates pericardial edema, which bursts in *blo/moda*. **(e-p)** Live DIC images of *blo/moda* embryos at 3 dpf highlighting the *moda* phenotypes in the fins and retina (e-h, arrows), in the otic vesicle and jaws (i-l, arrows) and in the tail (m-p), **(q-t)** *ath5:GFP* transgene expression in *blo/moda* embryos at 3 dpf. **(u-x)** TUNEL staining of *blo/moda* embryos at 3 dpf, highlighting apoptosis in the fins (red arrow) and CNS (blue arrow)

3.9 The *moda* mutation lies in a maternal effect gene

Since *moda* mutants develop completely normal until a specific stage and then gradually degenerate within a short time, the gene affected by the *moda* mutation may code for a maternally deposited factor and the phenotype manifests once this factor depletes during development.

This idea got strong support, when I investigated the *moda* phenotype in a different background.

So far I have only described the *moda* phenotype of embryos in the *AB/Ekw* background (methods 5.1). In the *LF/AB* background the *moda* phenotype is more severe than in the *AB/Ekw* background and mutants die 1 day earlier than those in the *AB/Ekw* background. Degeneration of the retina and CNS can already be observed at 2 dpf, hemorrhages are more frequent and some embryos exhibit ventricle expansion (Fig. 14d-f).

Interestingly, when crossing carriers in the *LF/AB* background with carriers in the *AB/Ekw* background the background of the female determines the severity of the *moda* phenotype. Mutant embryos coming from a *LF/AB* female and an *AB/Ekw* male exhibit the strong phenotype typical for the *LF/AB* background (Fig. 14j-l), whereby mutant embryos coming from an *AB/Ekw* female and a *LF/AB* male exhibit the mild phenotype typical for the *AB/Ekw* background (Fig. 14g-i). Thus, mutant offspring from a particular female carrier always exhibit a *moda* phenotype of similar severity; independent of the male carrier the female was paired to.

This observation strongly suggests that the *moda* phenotype is caused by loss of function of a maternal effect gene. Females in the *AB/Ekw* background may deposit a higher amount of the *moda* factor than females in the *LF/AB* background, which allows mutant offspring in the *AB/Ekw* background to develop normally for a longer period than mutants in the *LF/AB* background.

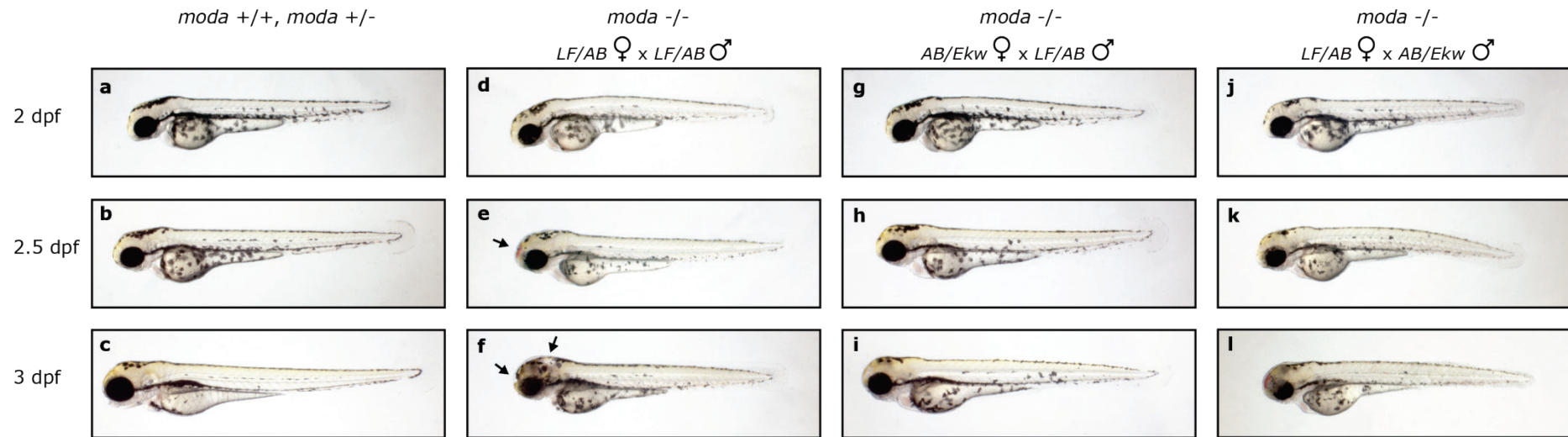


Figure 14: The female carrier determines the phenotype of mutant offspring. Live images of *moda* embryos at different stages (indicated on the left) with different parental backgrounds (indicated on top). Arrow in **e** indicates a ventricular hemorrhage, arrows in **f** indicate enlarged ventricles

3.10 The *moda* mutation maps to a 1.4Mb region on chromosome 16

In order to identify the gene affected by the *moda* mutation, I performed linkage mapping and was able to restrict the interval to a 1.4 Mb region on the upper arm of chromosome 16, between 2.88 Mb and 4.17 Mb (Fig. 15).

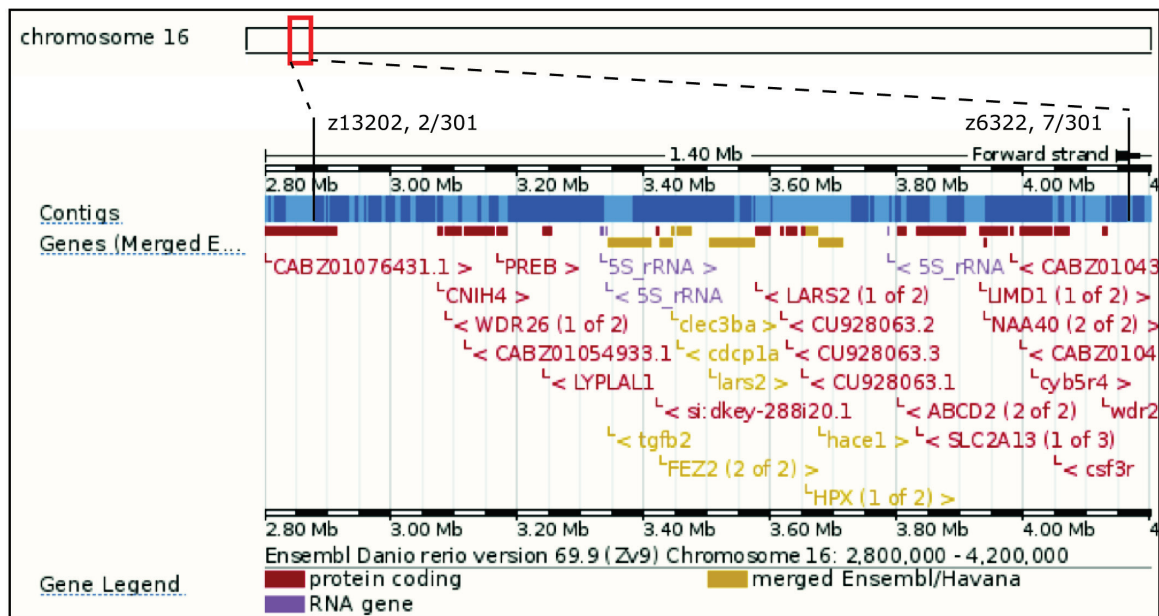


Fig. 15: The gene affected by the *moda* mutation maps to a 1.4 Mb region on chromosome 16. Markers defining the interval are shown above the interval together with the number of recombinants found for this particular marker. Image taken from ensembl.org on 15.03.2013.

4. Discussion

In the present study I have characterized a novel zebrafish mutant, which I termed *modern art* (*moda*). *Moda* mutants exhibit a pleiotropic phenotype involving degeneration of the retinal pigment epithelium and neural retina. Intriguingly, retinal degeneration only affects the dorso-anterior quadrant of the eye, while the ventral and posterior quadrants remain largely intact. To our current understanding, there are no functional or structural differences between different eye compartments that could explain a non-uniform retinal degeneration. I aimed to understand the cellular mechanisms that lead to this striking phenotype. I demonstrated that retinal degeneration in *moda* mutants is caused by a non-cell autonomous mechanism and that it is rescued by a loss of blood flow. The mutant locus maps to a 1.4 Mb region on the left arm of Chr 16, containing 20 candidate genes. Moreover, I discovered that the *moda* mutation lies in a maternal effect gene. Based on my current results I would like to propose three models that could explain retinal degeneration in *moda* mutants.

4.1 Cell death in the dorsal anterior brain and retina is likely caused by CSF that has leaked through the embryonic ependyma

Moda mutants exhibit severe degeneration in the brain and retina, which can be rescued by a loss of blood flow. In the brain, degeneration starts in the embryonic ependyma and progressively spreads to adjacent neuroepithelial areas, whereby at 3 dpf the dorsal anterior brain is most affected. I suggest that the increased apoptosis in the dorsal anterior brain is caused by excessive fluid that accumulates exactly in this brain area. Given that this fluid is distributed around the forebrain ventricle, I assume that it stems from the ventricular system. Apoptosis in the embryonic ependyma may impair its barrier properties, causing cerebrospinal fluid to enter the surrounding neural tissue.

While this seems to be case for the CNS, the situation in the retina may be more complex. I have shown that retinal degeneration is caused by a non-cell autonomous mechanism and that blood circulation is somehow, directly or indirectly, implicated in this phenotype. But how would this explain the regional differences of retinal degeneration along the dorso-ventral axis?

Retinal degeneration starts in the retinal pigment epithelium. Vascular defects, particularly increased permeability of choroidal blood vessels, have been reported to severely affect integrity of the retinal pigment epithelium and the neural retina [6, 58]. However, in 2 dpf zebrafish embryos, the choroidal capillary network, which supplies the RPE and outer retinal layers, has not yet developed. At this time, the eye is only supplied by a few vessels which line the surface of the retina, a few

vessels behind the lens and by the inner optic circle that connects the inner retinal vasculature with the outer vasculature^[18]. The relation between the RPE and the endothelium at this stage has not yet been described and even if one assumes a strong interaction, this early vasculature is patterned uniformly and therefore cannot explain why one side of the retina would be affected stronger than the rest. I would therefore not suggest that a vascular defect is a direct cause of retinal degeneration in *moda* mutants. Rather, the circulatory system may act indirectly by causing the structural failure of the ventricles detailed above, which in turn could lead to progressive tissue damage in the dorsal anterior brain and retina. It is telling that cell death affects primarily those retinal regions that are located closest to the forebrain ventricle.

At 3 dpf the entire retina stretches towards the direction of RPE loss. Loss of retina integrity due to RPE degeneration has already been described in other zebrafish mutants, resulting in mild deformation of the retina at sites of RPE loss. In some mutants that display defects in cell adhesion, including N-cadherin and laminin mutants, the central neural retina expels through the RPE into the forebrain^[53]. In *moda* mutants the stretching of the retina is rescued by loss of circulation and can therefore not be due to a loss of an adhesion or matrix protein essential for cell adhesion within the retinal tissue. I would rather suggest that loss of cell adhesion is a consequence of increased fluid accumulation in the retinal tissue. The retina then expands through a breakpoint where integrity of the tissue is weakest, namely through sites of RPE loss. Moreover, fluid accumulation in the brain could exert a physical pressure onto the retina and force retinal cells to squeeze between the skin epithelium and the brain.

4.2 Possible mechanisms that may lead to CNS degeneration in *moda* mutants

Based on the assumption that neuronal death in the dorsal anterior brain and retina is caused by a ventricular rather than a vascular defect, I will present three possible models to explain how ventricular function may be affected in *moda* mutants.

4.2.1 Model 1: Increased endothelial permeability impairs ependymal function

In *moda* mutants, apoptosis in the ependymal cell layer and adjacent neural tissues can be rescued by a loss of blood flow. A vascular defect is therefore a potential cause of cell death in the CNS. Vascular abnormalities that are observed in *moda* mutants include increased hemorrhaging in the brain and tail, the formation of cell clots in the circulation and the frequent obstruction of blood flow in small diameter vessels. All could be explained by decreased blood vessel integrity. A weak endothelium has a high probability of getting ruptured, leading to hemorrhage. Hemorrhaging activates the coagulation pathway, whereby blood clots form in order to reseal the endothelium. These clots may be subsequently transported via the blood stream to distant sites, where they may interrupt blood flow.

However, cell death in the ependymal cell layer precedes an observable vascular defect. Therefore, in order for this model to be plausible, a subtler vascular defect has to be present from early on. Increased blood vessel permeability may affect adjacent tissues including the ependymal cell layer. Various studies in mouse and chick suggest that the embryonic ependyma absorbs blood components on its abluminal side and secretes cerebrospinal fluid into the ventricular system already during early brain development ^[41, 59]. If the endothelium is leaky, the concentration of blood components on the abluminal side of the ependyma is increased and altered concentration gradients could then affect the transport dynamics of ependymal cells and cause cell death. Cell death in the embryonic ependyma would affect its barrier function; CSF may then enter the neural tissue and cause tissue damage. (Fig. 16b) Since the embryonic ependyma forms the ventricular barrier along the entire ventricular system, it is interesting to find fluid accumulation and tissue damage primarily in the vicinity of the forebrain ventricle. Maybe this could be explained by a denser association of blood vessels with the forebrain ventricle, compared to the mid- and hindbrain ventricles in 2 dpf zebrafish embryos^[18].

4.2.2 Model 2: The *moda* mutation directly affects ependymal function

Although apoptosis in the ependyma is rescued by a lack of blood flow, the *moda* mutation may still affect the embryonic ependyma directly rather than through the vasculature.

The embryonic ependyma plays a major role in ventricle expansion and CSF production, both of which are dependent on blood circulation^[34, 60]. As the ependymal cell layer forms the interface between blood and CSF, its task is to selectively transport molecules from one compartment to the other^[40]. Some blood-derived factors may be modified before they are released into the ventricular lumen as it is the case in the adult choroid plexus epithelium^[42]. In the absence of blood flow these capabilities including all proteins that function exclusively in these processes are dispensable. It is therefore possible that the *moda* mutation lies in a factor required for the homeostasis of transport across the ependyma and that its phenotype will not manifest if blood flow is absent.

In this model, the *moda* mutation either affects the vascular and ventricular system independently or vascular abnormalities result from an ependymal defect. Endothelial integrity may be affected in tissues that are highly apoptotic, leading to the appearance of hemorrhages in the brain. Cell clots that form to reseal the endothelium may be distributed in the entire circulatory system, thereby spreading the vascular defect from the CNS to the tail. Another possibility could be that the leakage of CSF into the surrounding tissue forces more water and small molecules to move from the vasculature into the ventricular lumen. Consequently the concentration of large molecules and cells in the vasculature increases, the blood thickens and cell clots form. These cell clots may clog small diameter vessels found in the brain and tail and obstruct blood flow. (Fig. 16c)

4.2.3 Model 3: The *moda* mutation mainly affects highly proliferating tissues due to early depletion of the maternal effect component

Maternal effect genes include all factors that are required for early embryonic development prior to the onset of zygotic gene transcription. These include factors important for cell division, protein synthesis, protein trafficking, cell-cell interactions, basic cell metabolism and factors that determine the dorsal-ventral and anterior-posterior axis of the embryo. All maternally deposited factors, excluding those that are involved in axis specification, are uniformly distributed in the nucleus and cytoplasm and after cell division they are equally distributed between daughter cells. Consequently, a maternal factor will deplete earlier in proliferating cells and later in cells that have become postmitotic after only a few divisions. Besides, cells that have a high metabolic rate may require a higher amount of a specific maternal factor^[61].

In *moda* mutants, one observes tissue degeneration in two highly proliferating tissues, the ventricular zone in the CNS and the fin primordium in the pectoral fins. As a loss of blood flow affects ventricle expansion and CSF production, neuronal stem cells proliferate to a much lesser extent in *bloated* mutants compared to siblings^[34, 62].

In *blo* mutants, the *moda* factor may therefore not deplete in the central nervous system until 4 dpf. A loss of blood flow does not affect fin development, which may explain why fin degeneration is not rescued in *blo* mutants.

In this third model the *moda* factor may encode any protein that is required for basic cellular functions. Cells that lose this essential factor ultimately undergo apoptosis. (Fig. 16c)

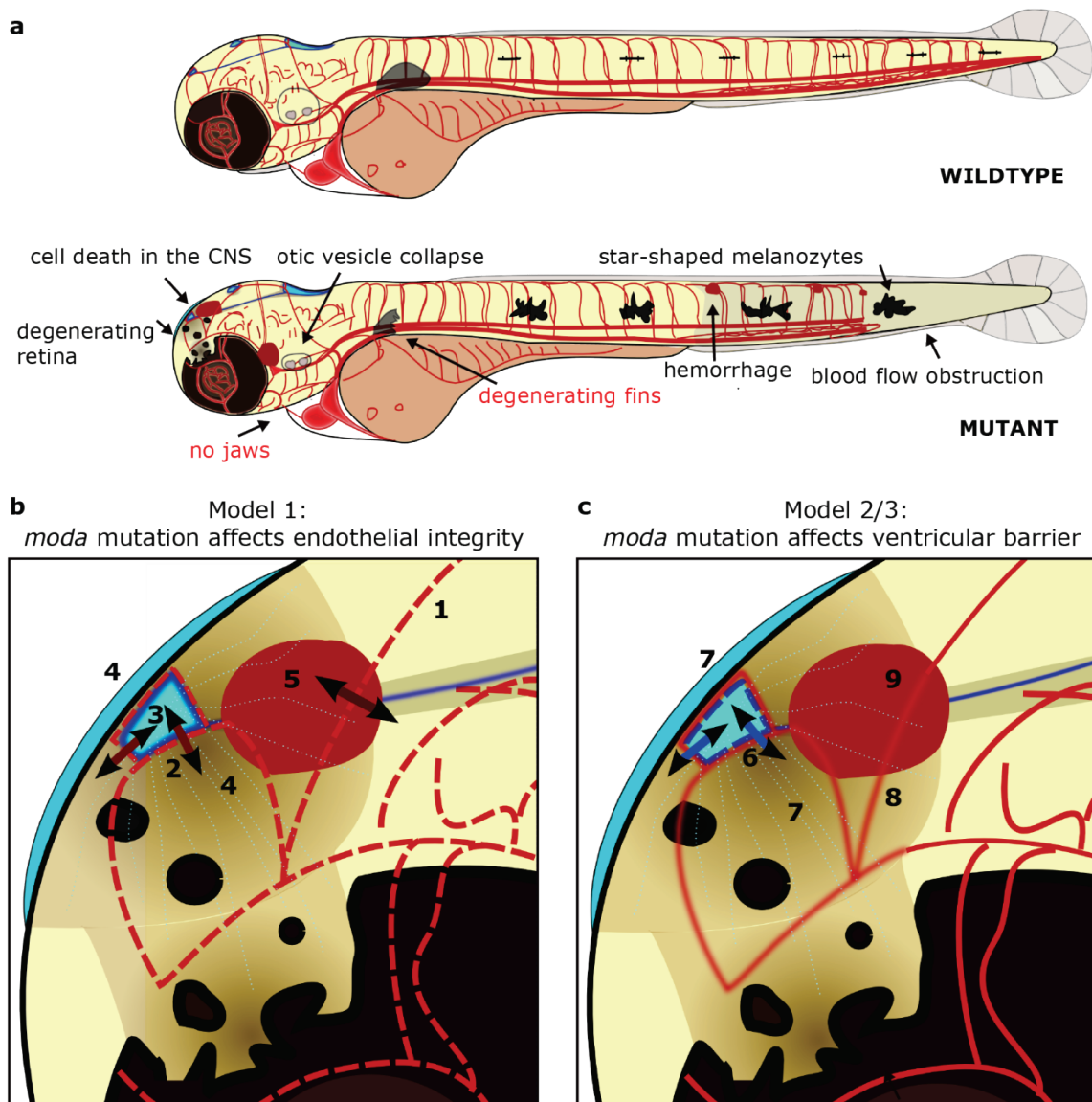


Figure 16: Potential causes for ventricular barrier disruption in *moda*. **(a)** Schematic summarizing the *moda* phenotype. Defects that are not influenced by a loss of blood flow are printed in red. The vascular system depicted in red corresponds to 2 dpf zebrafish embryos^[18], opaque areas indicate cell death. **(b)** Schematic of model 1: The *moda* mutation affects endothelial integrity leading to increased blood diffusion into the surrounding tissue (1). Increased concentration of blood components in the periventricular space causes cell death in the ependymal cell layer (2) and disruption of the ventricular barrier (3). Consequently, CSF leaks into the surrounding brain tissue (4). Moreover, hemorrhages occur in areas where the endothelium has become disrupted (5). **(c)** Schematic of model 2 and 3: The *moda* mutation affects the ventricular barrier (6) and causes CSF to leak into the surrounding brain tissue (7). The endothelium is either affected directly by the *moda* mutation or indirectly due to extensive apoptosis in the adjacent tissue (8). Moreover, hemorrhages occur in areas where the endothelium has become disrupted (9). Primary affected tissue is indicated by dashed lines (endothelium in model 1, ependyma in model 2), secondary affected tissue is indicated by blurred lines (ependyma in model 1, endothelium in model 2)

4.3 Similarities between the ventricle and the otic vesicle defect – requirement for ion channel regulation

The ventricle and otic vesicle defect share some common features in as much as that they both involve a loss of fluid from their enclosed lumen. Both the ventricles and the otic vesicle contain a fluid filled lumen, surrounded by a secretory epithelium. This secretory epithelium, consisting of ependymal cells in the ventricles and marginal cells in the inner ear, is associated with the vasculature and transports molecules from the circulation into the respective fluid compartment and vice versa. The epithelium's function is essential for the maintenance of fluid volume and composition and relies on the expression of numerous ion channels and related transport proteins. *Atp1a*, a Na-K-ATPase expressed in the ependyma, is required for ventricle inflation^[34]. *Nkcc1*, a Na-K-2Cl co-transporter expressed in marginal cells of the inner ear, is essential for the maintenance of endolymph volume^[63]. It is possible that both tissues are affected by the *moda* mutation by the same mechanism.

4.4 The mutant locus maps to the upper arm of Chromosome 16

The *moda* mutation maps to a 1.4 Mb region on the upper arm of chromosome 16. The Ensembl genome annotation project has identified 24 open reading frames in this region. Each ORF contains a ribosome binding site and is therefore potentially protein coding. Most of the genes have an allocated gene name and have already been described in a cellular or biochemical context. It should be noted that the candidate region is not well annotated. Some genes have been mapped (by Ensembl) to two or three different genomic locations and the actual location is unclear. Nevertheless I attempted to assess the possibility that one of these genes is the gene affected in *moda* mutants. As the *moda* phenotype is caused by loss of a maternal effect gene, one can assume that the *moda* mutation causes a loss of function of the affected protein. I collected information about the expression pattern during early vertebrate development, about phenotypical analysis of vertebrate knockout strains and about involvement in general cellular functions for each of the candidate genes. I exclude those genes that are not expressed prior to blastula stage, as they are not maternally deposited, and those that have been shown to cause a phenotype distinct from the *moda* phenotype if mutated or repressed. Table 1 lists all the candidate genes and their biological function.

I do not find an obvious candidate gene in this region. I therefore favor an uncharacterized protein to be mutated in *moda*. Two genes in the interval have been identified as WD-repeat proteins; their cellular functions are however unknown. Repeated WD motifs act as a site for protein-protein interaction, and proteins containing WD repeats are known to serve as platforms for the assembly of protein

complexes. Members of this class of proteins are involved in multiple cellular functions that include signal transduction, RNA processing, cytoskeletal assembly and vesicle trafficking^[64]. Loss of function mutations in these genes may therefore lead to a wide spectrum of phenotypes.

Lypophospholipase-like 1 (Lyplal 1) and N α -acetyltransferase 40 (Naa40) are zygotically expressed^[65] and are therefore potential candidate genes. Moreover, Lyplal1 has been implicated in ion channel regulation in HEK293 cells^[66]. If Lyplal1 performs the same cellular function in zebrafish, its loss may affect the ventricles and the otic vesicle as observed in *moda* mutants.

It should be noted, that the *moda* phenotype may be caused by more than one mutation. Given that ENU treatment causes multiple point mutations per sperm cell, it is possible that two or more genes were mutated that are genetically linked and therefore always co-segregate during meiosis. However, I find that the expressivity of all different phenotypes correlates, such that in embryos that display comparably early CNS degeneration the jaws do not develop at all, while in embryos that display comparably late CNS degeneration the jaws develop but are strongly reduced. This makes it unlikely that the *moda* phenotype is caused by two closely linked mutations.

Gene name and molecular/cellular function according to GO	expression pattern, gene knockdown, additional biological functions
<u>Cornichon homologue 4</u> (cni4) Cnih: intracellular signal transduction, membrane bound	No data about expression and gene knock down Paralogue <i>cni4</i> zygotically expressed ^[65] , <i>cni4</i> -2/-3 important for AMPA receptor regulation in murine neurons ^[67]
! <u>WD-repeat protein 26</u> (wdr26)	No data about expression and gene knock down
<u>Prolactin- regulatory element binding</u> (PREB, zgc:92203) Transcription factor activity	Expressed from gastrula stage ^[68] , not expressed prior to E10.5 in mice ^[69] , no maternal effect component
! <u>Lipophospholipase-like 1</u> (Lypl1, zgc:110848) Hydrolase activity, acyl thioesterase activity [70]	Zygotically expressed ^[65] , controls surface expression of calcium activated ion channels in HEK293 cells ^[70]
<u>Transforming growth factor b2</u> (tgfb2) Growth factor activity, palate development	Expressed from bud- stage ^[71] , MO- knockdown causes a phenotype different from <i>moda</i> ^[72]
<u>si:dkey-288i20.1</u> Thiolester hydrolase activity, Acyl-CoA metabolic process	No data about expression and gene knock down
<u>Fasciculation and elongation protein zeta 2</u> (FEZ2, si:dkey-288i20.2)	No data about expression and gene knock down C.elegans homolog is involved in axonal outgrowth and fasciculation ^[73]
<u>C-type lectin domain family 3, member Ba</u> (Clec3ba) carbohydrate binding	No data about expression and gene knock down Clec14a expressed from 1-somite stage, <i>clec16a</i> zygotically expressed ^[65]
<u>CUB-domain containing protein 1a</u> (Cdcp1a)	No data about expression and gene knock down, human homologue <i>cdcp1</i> is overexpressed in various cancer types. transmembrane protein that regulates cell survival, cell adhesion, cell migration, angiogenesis ^[74]
<u>Leucine t-RNA synthetase</u> (Lars2) Leucyl, tRNA aminoacylation, mitochondrial	No data about expression and gene knock down Likely maternally deposited given its essential role during protein synthesis
<u>Hemopexin</u> (HPX, zgc:152945) Metal-ion binding	No data about expression and gene knock down, plasma protein that binds heme, antioxidant action by binding free heme in extracellular space ^[75]

Gene name and molecular/cellular function according to GO	expression pattern, gene knockdown, additional biological functions
<u>HECT domain containing ubiquitin ligase 1</u> (Hace1) Upiquitin-protein ligase activity	No data about expression and gene knock down important for reestablishment of golgi after cell division in yeast ^[76] , given this important function it may be maternally deposited, inhibits RohGTPases and thereby regulates cell cycle, motility and cell-cell adhesion, tumor suppressor ^[77]
<u>ATP-binding cassette sub-family 2</u> (ABCD2)	No data about expression and gene knock down Member of ALD subfamily, which is involved in peroxisomal import of fatty acids, mutations are associated with adrenoleukodystrophy in humans ^[78]
<u>solute carrier family 2, member 13</u> (SLC2A13) Glucose transmembrane transporter activity	No data about expression and gene knock down large family of proteins, 22 SLC2A glucose transporters identified in zebrafish, two of them are zygotically expressed, for 17 of those expression cannot be detected prior to blastula stage ^[79] , MO-knockdown of SLC2A1a causes apoptosis in the CNS ^[80]
<u>LIM protein domain 1</u> (LIMD1)	No expression data, Limd -/- mice viable ^[81] , MO-knockdown of Limd1a causes a phenotype different from <i>moda</i> ^[81, 82]
! <u>Nα-acetyltransferase 40</u> (Naa40) N-acetyltransferase activity	Zygotically expressed, ubiquitously expressed in 1dpf embryos ^[65] , no data about cellular function
<u>Cytochrome b5 reductase 4</u> (Cyb5r4) Oxidoreductase activity, located in endoplasmic reticulum	No expression data for early embryonic development, at 36 hpf expressed in blood and vasculature ^[83]
<u>colony stimulating factor 3 receptor</u> (Csf3r) Cytokine receptor activity, granulocyte differentiation	Expressed from the 5-somite stage in blood islands ^[84] , not maternally deposited
! <u>WD-repeat protein 21</u> (wdr21)	No data
3 uncharacterized open reading frames CABZ01054933, CU928063, CABZ01043951	No data

Table 1: *Moda* candidate genes and their biological function. Mutations in genes that are written in grey are unlikely to be responsible for the *moda* phenotype. Genes that are highlighted by ! are the best candidates.

4.5 Future directions

Which gene is mutated in *moda* and where is it expressed?

The identification of the mutant locus would aid our understanding of the *moda* phenotype. Only with the affected gene in hand I would be able to investigate the expression pattern of the *moda* factor and its molecular functions.

Does the *moda* mutation affect ependymal and/or vascular integrity?

My working hypotheses argue that the endothelium and/or the ependyma lack integrity. In order to investigate endothelial and ependymal permeability I want to inject a dye into the circulation and ventricular system, respectively, and assess the capability of the respective cell layer to prevent diffusion of the dye. If increased endothelial permeability results in ependymal cell death, I should be able to detect a high diffusion rate of the dye across the endothelium as early as 2 dpf. This method would also enable us to define the origin of excessive fluid in the brain. If the fluid in the anterior brain stems from the forebrain ventricle, I should be able to detect staining of the anterior brain if a dye was injected into the ventricular system and not if a dye was injected into the blood circulation.

Is cell death in the ependyma caused by a cell autonomous or non-cell autonomous mechanism?

In order to investigate whether the ependyma is directly (model 2) or indirectly (model 1) affected by the *moda* mutation, I want to perform transplantation experiments. A mutant transplant that forms a large part of the ependyma in a wildtype background should cause a phenotype if cell death is caused by a cell autonomous mechanism and should not cause a phenotype if cell death is the result of a non-cell autonomous factor.

5. Materials and Methods

5.1 ENU mutagenesis and zebrafish strains

AB and *tup LF* wild-type, *AB tg(ath5:GFP)*, *tup LF tg(PU1:RFP)* and *modern art (moda)* zebrafish (*Danio rerio*) strains were bred and maintained according to standard procedures^[85]. Collected embryos were reared in E3 embryo medium (5.0mM NaCl, 0.17mM KCl, 0.33mM CaCl, 0.33mM MgSO₄, 0.05% methylene blue) at 28.5 °C, if not otherwise indicated. Embryos used for fluorescent imaging were raised in E3 containing 0.003% PTU (Sigma Aldrich) from 22hpf.

ENU mutagenesis was performed in the *AB* background, mutagenized male fish were crossed to an *AB* female, individual offspring were outcrossed to the *Ekwill* background and families were generated. In the course of this study *moda* carriers were outcrossed to different transgenic lines in different backgrounds, which is schematized in Fig. 17.

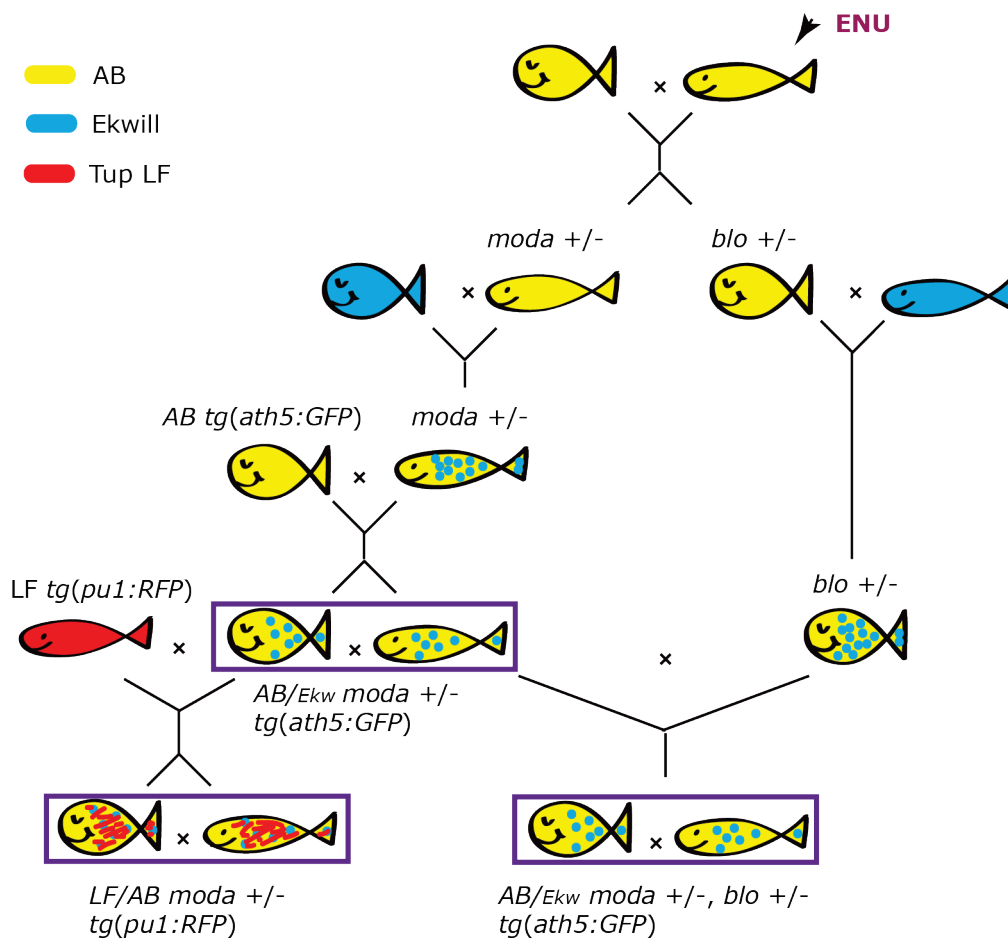


Fig.17: Schematic of *moda* outcrosses. ENU mutagenesis was performed in the AB background, ENU treated males were crossed to untreated AB females and offspring were outcrossed to the Ekwill background. Offspring, carrying the *moda* mutation, were crossed to the AB *tg(ath5:GFP)* transgenic line. In order to investigate the *moda* mutation in a *pu1:RFP* transgenic background, *moda* carriers from the AB/Ekwill *tg(ath5:GFP)* background were crossed to the Tup LF *tg(pu1:GFP)* line. Moreover, in order to generate circulation deficient *moda* mutants, AB/Ekw *tg(ath5:GFP)* *moda* carriers were crossed to AB/Ekw *blo* carriers, which were isolated from the same ENU mutagenesis screen. Different backgrounds are differently colored as shown on the top left. Boxed couples were frequently incrossed to generate homozygous mutants. Live images of embryos from boxed breeding couples are shown in Fig.1 (*AB/Ekw tg(ath5:GFP) moda*), Fig.13 a-d (*AB/Ekw tg(ath5:GFP) blo/moda*) and Fig.15 (*AB/LF tg(pu1:RFP) moda*), respectively. Embryos from the boxed couple *AB/Ekw tg(ath5:GFP) moda* were used for most experiments.

Taq-Polymerase (Invitrogen) and the primers listed in Fig.18b. The reverse primers include a T3- promoter sequence to allow direct in vitro transcription from the PCR product. PCR amplification was performed in a mixture of 50µl containing 5µl 10x PCR buffer (Invitrogen), 1.5µl 100mM MgCl₂ (Invitrogen), 1µl 10µM Primer F, 1µl 10 µM Primer R, 1µl 10µM dNTPs and 0.4µl Taq polymerase (Invitrogen) using the PRC program as follows: step 1. 95°C for 5 min, step 2. 95°C for 30 sec, step 3. 56°C for 30 sec, step 4. 70°C for 1 min, steps 2-4 x 40, step 5. 70°C for 10 min, 4°C forever. The PCR product was purified according to the QIAgen PRC purification kit. In vitro transcription was performed according to the following protocol:

The following reagents were added to a 0.2ml microcentrifuge tube:

2 ng template DNA

2 µl DIG-mix (Roche)

4 µl 5x transcription buffer (Promega)

2 µl T3 RNA polymerase (Promega)

2 µl 100mM DTT (Promega)

0.5 µl RNAsin (Promega)

topped up with ddH₂O to a final volume of 20 µl.

The reaction was performed for 2hr at 37°C.

In order to degrade the DNA template 1 µl of DNase (Roche 10000u) was added to the reaction tube and the tube was incubated for additional 20 min at 37°C.

The RNA was purified by applying the reaction mixture twice to an "illustra ProbeQuant G-50 Micro Column" provided by GE Healthcare Life Sciences.

Embryo fixation

Embryos were dechorionated, anesthetized with 40µl Tricaine 25x (0.8g/l Tricaine, Sigma A5040, 50mM Tris pH9.5) per ml embryo medium and then fixed in 4%PFA in PBST (0.1% Tween in 1xPBS) over night at 4°C. The following day embryos were first washed several times in 0.1% PBST, dehydrated into Methanol in sequential steps (25% MeOH in PBST, 50% MeOH in PBST, 75% MeOH in PBST, 100%MeOH) and stored over night or longer (up to 2 weeks) at -20°C.

RNA-hybridization

Embryos were step-wise rehydrated from MeOH into PBST and permeabilized via Proteinase K digestion. The duration of Proteinase K digestion depends on the age of the embryos shown in Table 2. The concentration of Proteinase K (Sigma P6556) was 10µg/ml PBST.

To stop the reaction embryos were washed several times in PBST and refixed for 20 min in 4% PFA (4%PFA in PBST) at RT. PFA was removed and the embryos were washed in PBST. For prehybridization, embryos were incubated for at least 2 hours in Hyb+ (5x SSC, 50% formamide, 0.1% Triton, torula, RNA, heparin) at 68°C. The

DIG-labelled RNA probe was diluted in Hyb+ and different concentrations of probe were tested to determine the optimal probe concentration (good signal to background ratio). Hybridization was performed over night at 68°C.

The following day the probe in Hyb+ was taken off and stored for reuse at -20°C. The embryos were washed 4x for 30 min in Hyb+, 15 min in 2x SSC (300mM NaCl, 30mM Na₃Citratex2H₂O) and 2x 30 min in 0.2x SSC at 68°C. Embryos were rinsed a few times in PBST and washed over one hour with several changes in PBST at RT.

Probe detection using an α - digoxigenin antibody

For blocking, embryos were incubated for at least an hour at RT in 5% MABlock (0.5M maleic acid, 0.5M NaCl, pH 7.5, 2% goat serum, 2mg/ml BSA). The α -digoxigenin antibody conjugated with an alkaline phosphatase (Anti-Digoxigenin-AP Fab fragments, Roche Diagnostics, 150U) was diluted 1:6000 in 5% MABlock and added to the embryos. Antibody binding was performed over night at 4°C.

Alkaline Phosphatase reaction

The antibody was removed and the embryos were washed over one hour in PBST (4x 15min) and afterwards 3x for 5min in Xpho-buffer (0.1M Tris HCl pH 9.5, 50mM MgCl₂, 0.1M NaCl, 0.1% Triton-X100). 1 μ l NBT and 3.5 μ l BCIP were added to 1ml Xpho and added to the embryos. The alkaline phosphatase reaction took place over night at RT in the dark. As soon as a clear signal could be observed the embryos were washed in PBST and post-fixed in 4% PFA over night at 4°C.

Somites/ hpf	In situ hybridization Duration in min	Antibody staining Duration in min
5s	1	0
10-15s	3	1
20s	10	2
24 hpf	10	10
30 hpf	22	20
48 hpf	30	30
55 hpf	38	45
72 hpf	50	60

Table 2: Proteinase K digestion to permeabilize fixed zebrafish embryos. Left column: developmental stage of embryos, middle column: duration of PK digestion for in situ hybridization, right column: duration of PK digestion for antibody staining

5.3 Wholemout antibody staining

Embryos were dechorionated and then fixed in 4%PFA over night at 4°C. The following day embryos were washed in PBST, step-wise dehydrated into Methanol and stored over night or longer (up to 2 weeks) at -20 degree. For brain structure analysis, brains were dissected prior to dehydration into methanol.

Antibody binding

Embryos/brains were step-wise rehydrated from MeOH into PBST and permeabilized via Proteinase K digestion. The duration of Proteinase K reaction depends on the age of the embryos (Table 2). Dissected brains were always digested for 10 min independent of the age of the embryo. The concentration of Proteinase K (Sigma P6556) was 10µg/ml PBST. To stop the reaction embryos were washed several times in PBST and refixed for 20 min in 4% PFA. PFA was removed and the embryos were washed in PBST. For blocking, embryos were incubated for 2 hours at RT in IB (1% NGS, 0.1% DMSO, 0.1% Triton in PBS). The primary antibody was added to IB and antibody binding was performed over night at 4°C. Primary and secondary antibodies used in this study and their concentrations during antibody binding are shown in Table 2. The following day the primary antibody was removed, the embryos were washed over 4hr with several changes in PBST at RT and the secondary antibody was added. Embryos were incubated in the secondary antibody over night at 4°C.

The following day the secondary antibody was removed and embryos were washed for 2hr or longer at RT in PBST. Imaging was performed using confocal imaging (Leica TCS SP8 X).

Antibody	dilution	reference
<u>Primary antibodies</u>		
α-acetylated tubulin, mouse IgG2b	1:500	Sigma
α-SV2, mouse IgG1	1:200	Developmental Studies Hybridoma Bank
α-Lcp1 (IN), Z-fish, rabbit IgG	1:50	Anaspec
α-BrdU, mouse	1:400	Sigma
<u>Secondary antibodies</u>		
Biotinylated antibody, α-rabbit IgG	1:200	Vectastain
α- mouse IgG1, Alexa 633	1:200	Invitrogen
α- mouse IgG2b, Alexa 568	1:200	Invitrogen
α- mouse IgG, Alexa 568	1:1000	Invitrogen
α- digoxigenin-AP Fab fragments	1:6000 -in situ 1:3000 -TUNEL	Roche

Table 2: List of antibodies used in this study

5.4 TUNEL staining

Embryos were fixed for 3hr in 4% PFA at RT, washed several times in PBSTr (0.8% Triton X-100 in 1xPBS) and step-wise dehydrated into Methanol. Embryos were kept for 1 week at -20°C before proceeding with the protocol.

Embryos were rehydrated from Methanol into PBSTr and permeabilized by PK digestion (20µg per ml PBSTr), which was performed for 55 minutes at RT for 50dpf embryos, for 60 minutes for 58hpf embryos and for 70 minutes for 66hpf embryos. Embryos were rinsed carefully in PBSTr and immediately postfixed in 4% PFA for 20 min at RT. PFA was removed and embryos were washed over 15 minutes with a few changes in PBSTr at RT. Subsequently, embryos were incubated for 10 min. in prechilled ETOH: Acetone 2:1 at -20°C followed by several washes in PBSTr. The terminal deoxynucleotidyl transferase reaction was performed according to the ApopTag Kit, Chemicon International.

The following day the reaction mixture was discarded and the embryos were washed for 1h in PBSTr at RT, blocked for 2hr in 5% MaBlock and incubated over night in 5% MABlock containing α - digoxigenin antibody conjugated with an alkaline phosphatase diluted 1:3000. Alkaline phosphatase reaction was performed as described in section 5.2.

5.5 Inhibition of Apoptosis

To inhibit p53 expression, one-cell staged embryos obtained from *moda*^{+/-} incrosses were injected with 10 nl of 1 mM p53MO (5'-GCGCCATTGCTTTGCAAGAATTG-3'; GeneTools). For each individual p53MO experiment, embryos from the same clutch were used as experimental subjects.

To inhibit caspase activity, embryos were treated with Caspase inhibitor (Caspase Inhibitor Set IV, Calbiochem, 218825-1SET) according to the manufacturer's protocol from 36hpf until fixation.

5.6 BrdU staining

3 dpf embryos were incubated in 10mM BrdU (Sigma Aldrich), 15% DMSO in 1x E3 embryo medium (5.0mM NaCl, 0.17mM KCl, 0.33mM CaCl, 0.33mM MgSO₄, 0.05% methylene blue) for 30 min on ice. Embryos were washed for 1h at 28.5°C in 1x E3, subsequently fixed in 4% PFA over night at 4°C, step-wise transferred into 100% MeOH and stored at -20°C over night. Embryos were rehydrated in PBST followed by Proteinase K treatment (10µg/ml in PBST) for 25 min. After washing in PBST, embryos were postfixed in 4% PFA for 30 min, again washed over 30 min at RT and incubated in 2N HCL for 2x 10 min. Following several washing steps in PBST embryos were incubated for 1hr in blocking solution (1% NGS, 0.1% DMSO, 0.1% Triton in PBS) at RT and incubated over night in α -BrdU antibody (Table 2) diluted 1:400 in

blocking solution at 4°C. The primary antibody was removed and the embryos were washed over several hours in PBST. The secondary α -mouse antibody (Table 2) was added and the embryos were incubated overnight at 4°C. Embryos were counterstained with DAPI (Calbiochem, 1 μ g/ml PBST) for 3 hours at RT.

5.7 Cell transplantation experiments

Embryos from *moda*^{+/-} incrosses were injected with Histon2B-RFP mRNA (40-50 pg per embryo) at the one-cell stage. *Moda* embryos and *ABxTupLF* wildtype embryos were allowed to develop until the late blastula stage (high to sphere). In the late blastula stage, approximately 50 RFP⁺ cells were transplanted from the apical region of *moda* embryos (donor) into the most dorsal region of *ABxTupLF* wildtype (acceptor) embryos, the region that is fated to become the neural plate. Donor embryos were grown until 3 dpf to distinguish *moda* homozygous mutants from siblings and assess whether a particular acceptor embryo harbors a mutant or wildtype transplant. Acceptor embryos were imaged and fixed at 4dpf.

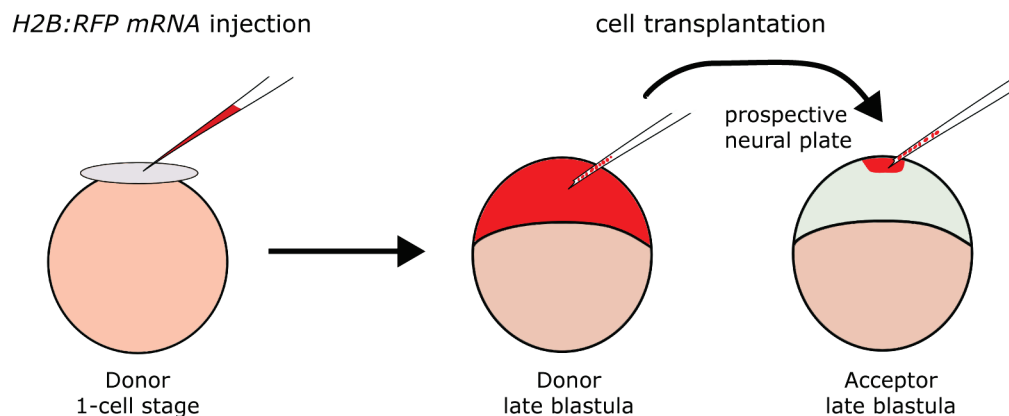


Fig. 18: Cell transplantation assay. Donor embryos were injected in the 1-cell stage with *H2B:RFP* mRNA (left), during blastula stage H2B:RFP positive cells were transplanted from donor embryos into the prospective neural plate of acceptor embryos.

5.8 JB-4 sections

Embryos were fixed over night at 4°C, rinsed a few times in PBST, washed over 30 minutes with several changes at RT in milliQ H₂O and dehydrated step-wise into Ethanol (30% Ethanol in milliQ, 50% EtOH on milliQ, 70% EtOH in milliQ, 95% EtOH in milliQ, 100% Ethanol). 0.36g of 'JB-4 catalyst' was added to 25ml of 'JB-4 solution A' (Sigma Aldrich EM0100), referred to as 'activated solution A'. Embryos were first incubated in a 1:1 mix of 'activated solution A' and 100% Ethanol for 1hr at RT and then in 100% 'activated solution A' over night at 4°C. Embryos were transferred to the coffin and the resin was prepared by adding 250µl of 'JB-4 solution B' (Polysciences) to 750µl of 'activated solution A'. Activated solution A was removed from the embryos and the resin was added. Embryos were quickly oriented and stored at RT until the resin has hardened. Samples were mounted on a microtome block and sectioned with a Leica Microtome. Sections were then stained with toluidine blue for 5 min ^[87].

5.9 Alcain blue staining

Embryos were step-wise dehydrated into 70% Ethanol and incubated over night at 4°C in a solution containing 4.5% Alcain blue, 70%Ethanol and 120 mM MgCl₂. Embryos were washed in PBST and imaged with a light microscope as described above.

5.10 β-Galactosidase-assay

The β-Galactosidase assay was performed as described by Kishi and colleagues in 2008 ^[57].

5.11 Mapping the *moda* mutation

The *moda* mutation was mapped by linkage mapping using amplified fragment length polymorphisms from the MGH panel (Zebrafish SSR search). Primer sequences to amplify those polymorphisms can be downloaded from <http://danio.mgh.harvard.edu/bacmarkers/ssr.html>. Fragments were amplified by Taq polymerase (Sigma) using the PCR protocol as follows: step 1. 95°C for 5 min, step 2. 95°C for 30 sec, step 3. 56°C for 30 sec, step 4. 70°C for 30 sec, steps 2-4 x 40, step 5. 70°C for 10 min, 4°C forever, and separated by gel electrophoresis using a 3% agarose gel in 0.5x TBE buffer.

5.12 DIC time lapse imaging

The imaged embryo was raised at 28.5°C until 2.4 dpf, anesthetized with 1x tricaine and embedded in 1% agarose in E3 1x tricaine. I selected for a comparably healthy embryo, which already showed RPE degeneration at 2.4 dpf. The chamber temperature during imaging was 32°C. I imaged for 24hr making an image every 2 minutes with a Leica DIC microscope.

5.13 Imaging and data processing

Embryos subjected to whole-mount in situ hybridization were cleared in serial incubations of glycerol (25, 50, 75 and 95%), cover-slipped, and imaged with a 40× (0.8 NA) water-immersion lens using a Nikon E1000 microscope connected to a digital camera (Jenoptik) operated by Openlab (Improvision) software. JB-4 sections were covered with DPX mounting medium (BDH), cover-slipped and imaged as above. Transgenic living embryos and whole-mount immunostained embryos were embedded in 1% Agarose in 1xE3; living embryos were additionally anesthetized with 1x tricaine in E3. They were imaged using a 40× (0.8 NA) water-immersion lens or 10x dry lens. All confocal images were processed using Volocity (Improvision) software and exported as tiffs. All figures were composed with Photoshop and Illustrator (CS5, Adobe).

6. References

1. Fadool, J.M. and J.E. Dowling, *Zebrafish: a model system for the study of eye genetics*. Progress in retinal and eye research, 2008. **27**(1): p. 89-110.
2. Gestri, G., B.A. Link, and S.C. Neuhauss, *The visual system of zebrafish and its use to model human ocular diseases*. Developmental neurobiology, 2012. **72**(3): p. 302-27.
3. Avanesov, A. and J. Malicki, *Approaches to study neurogenesis in the zebrafish retina*. Methods in cell biology, 2004. **76**: p. 333-84.
4. Stenkamp, D.L., *Neurogenesis in the fish retina*. International review of cytology, 2007. **259**: p. 173-224.
5. Strauss, O., *The retinal pigment epithelium in visual function*. Physiological reviews, 2005. **85**(3): p. 845-81.
6. Simo, R., et al., *The retinal pigment epithelium: something more than a constituent of the blood-retinal barrier--implications for the pathogenesis of diabetic retinopathy*. Journal of biomedicine & biotechnology, 2010. **2010**: p. 190724.
7. Ellertsdottir, E., et al., *Vascular morphogenesis in the zebrafish embryo*. Developmental biology, 2010. **341**(1): p. 56-65.
8. Lammert, E. and J. Axnick, *Vascular lumen formation*. Cold Spring Harbor perspectives in medicine, 2012. **2**(4): p. a006619.
9. Jin, S.W., et al., *Cellular and molecular analyses of vascular tube and lumen formation in zebrafish*. Development, 2005. **132**(23): p. 5199-209.
10. Pardanaud, L., F. Yassine, and F. Dieterlen-Lievre, *Relationship between vasculogenesis, angiogenesis and haemopoiesis during avian ontogeny*. Development, 1989. **105**(3): p. 473-85.
11. Gariano, R.F., *Cellular mechanisms in retinal vascular development*. Progress in retinal and eye research, 2003. **22**(3): p. 295-306.
12. Jin, S.W., et al., *A transgene-assisted genetic screen identifies essential regulators of vascular development in vertebrate embryos*. Developmental biology, 2007. **307**(1): p. 29-42.
13. Herbert, S.P., et al., *Arterial-venous segregation by selective cell sprouting: an alternative mode of blood vessel formation*. Science, 2009. **326**(5950): p. 294-8.
14. Lawson, N.D. and B.M. Weinstein, *Arteries and veins: making a difference with zebrafish*. Nature reviews. Genetics, 2002. **3**(9): p. 674-82.

15. Saint-Geniez, M. and P.A. D'Amore, *Development and pathology of the hyaloid, choroidal and retinal vasculature*. The International journal of developmental biology, 2004. **48**(8-9): p. 1045-58.
16. Alvarez, Y., et al., *Genetic determinants of hyaloid and retinal vasculature in zebrafish*. BMC developmental biology, 2007. **7**: p. 114.
17. Kitambi, S.S., et al., *Small molecule screen for compounds that affect vascular development in the zebrafish retina*. Mechanisms of development, 2009. **126**(5-6): p. 464-77.
18. Isogai, S., M. Horiguchi, and B.M. Weinstein, *The vascular anatomy of the developing zebrafish: an atlas of embryonic and early larval development*. Developmental biology, 2001. **230**(2): p. 278-301.
19. Butler, M.G., A.V. Gore, and B.M. Weinstein, *Zebrafish as a model for hemorrhagic stroke*. Methods in cell biology, 2011. **105**: p. 137-61.
20. Miano, J.M., et al., *Ultrastructure of zebrafish dorsal aortic cells*. Zebrafish, 2006. **3**(4): p. 455-63.
21. Ballabh, P., A. Braun, and M. Nedergaard, *The blood-brain barrier: an overview: structure, regulation, and clinical implications*. Neurobiology of disease, 2004. **16**(1): p. 1-13.
22. Simionescu, M., N. Simionescu, and G.E. Palade, *Segmental differentiations of cell junctions in the vascular endothelium. The microvasculature*. The Journal of cell biology, 1975. **67**(3): p. 863-85.
23. Bazzoni, G. and E. Dejana, *Endothelial cell-to-cell junctions: molecular organization and role in vascular homeostasis*. Physiological reviews, 2004. **84**(3): p. 869-901.
24. Dejana, E., F. Orsenigo, and M.G. Lampugnani, *The role of adherens junctions and VE-cadherin in the control of vascular permeability*. Journal of cell science, 2008. **121**(Pt 13): p. 2115-22.
25. Grazia Lampugnani, M., et al., *Contact inhibition of VEGF-induced proliferation requires vascular endothelial cadherin, beta-catenin, and the phosphatase DEP-1/CD148*. The Journal of cell biology, 2003. **161**(4): p. 793-804.
26. Carmeliet, P., et al., *Targeted deficiency or cytosolic truncation of the VE-cadherin gene in mice impairs VEGF-mediated endothelial survival and angiogenesis*. Cell, 1999. **98**(2): p. 147-57.
27. Montero-Balaguer, M., et al., *Stable vascular connections and remodeling require full expression of VE-cadherin in zebrafish embryos*. PloS one, 2009. **4**(6): p. e5772.

28. Corada, M., et al., *Vascular endothelial-cadherin is an important determinant of microvascular integrity in vivo*. Proceedings of the National Academy of Sciences of the United States of America, 1999. **96**(17): p. 9815-20.
29. Liebner, S., et al., *Claudin-1 and claudin-5 expression and tight junction morphology are altered in blood vessels of human glioblastoma multiforme*. Acta neuropathologica, 2000. **100**(3): p. 323-31.
30. Risau, W. and H. Wolburg, *Development of the blood-brain barrier*. Trends in neurosciences, 1990. **13**(5): p. 174-8.
31. Rizzolo, L.J., et al., *Integration of tight junctions and claudins with the barrier functions of the retinal pigment epithelium*. Progress in retinal and eye research, 2011. **30**(5): p. 296-323.
32. Colas, J.F. and G.C. Schoenwolf, *Towards a cellular and molecular understanding of neurulation*. Developmental dynamics : an official publication of the American Association of Anatomists, 2001. **221**(2): p. 117-45.
33. Folgueira, M., et al., *Morphogenesis underlying the development of the everted teleost telencephalon*. Neural Dev. **7**: p. 32.
34. Lowery, L.A. and H. Sive, *Initial formation of zebrafish brain ventricles occurs independently of circulation and requires the nagie oko and snakehead/atp1a1a.1 gene products*. Development, 2005. **132**(9): p. 2057-67.
35. Chang, J.T., L.A. Lowery, and H. Sive, *Multiple roles for the Na,K-ATPase subunits, Atp1a1 and Fxyd1, during brain ventricle development*. Developmental biology, 2012. **368**(2): p. 312-22.
36. Alonso, M.I., et al., *Disruption of proteoglycans in neural tube fluid by beta-D-xyloside alters brain enlargement in chick embryos*. The Anatomical record, 1998. **252**(4): p. 499-508.
37. Miyan, J.A., M. Nabiyouni, and M. Zendah, *Development of the brain: a vital role for cerebrospinal fluid*. Canadian journal of physiology and pharmacology, 2003. **81**(4): p. 317-28.
38. Desmond, M.E. and A.G. Jacobson, *Embryonic brain enlargement requires cerebrospinal fluid pressure*. Developmental biology, 1977. **57**(1): p. 188-98.
39. Parvas, M., C. Parada, and D. Bueno, *A blood-CSF barrier function controls embryonic CSF protein composition and homeostasis during early CNS development*. Developmental biology, 2008. **321**(1): p. 51-63.
40. Martin, C., et al., *FGF2 plays a key role in embryonic cerebrospinal fluid trophic properties over chick embryo neuroepithelial stem cells*. Developmental biology, 2006. **297**(2): p. 402-16.

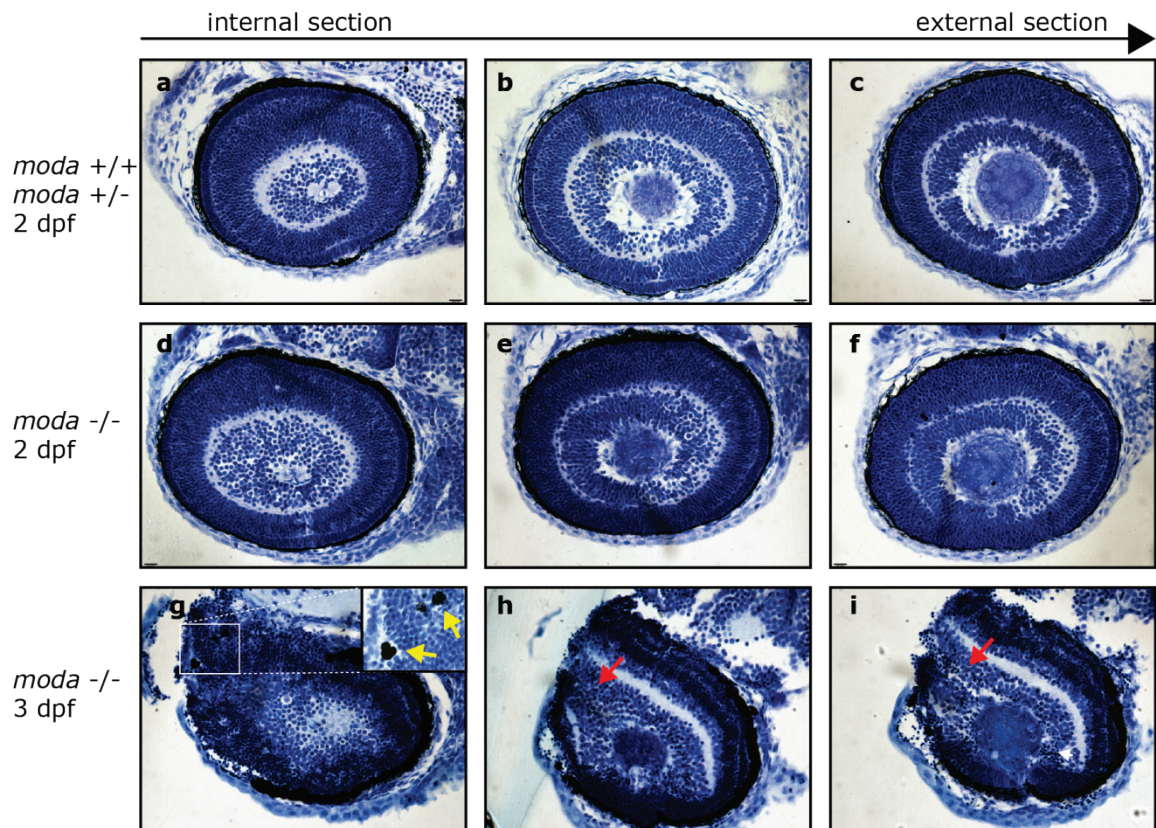
41. Parada, C., et al., *Proteome analysis of chick embryonic cerebrospinal fluid*. *Proteomics*, 2006. **6**(1): p. 312-20.
42. Redzic, Z.B. and M.B. Segal, *The structure of the choroid plexus and the physiology of the choroid plexus epithelium*. *Advanced drug delivery reviews*, 2004. **56**(12): p. 1695-716.
43. Turner, M.H., J.F. Ullmann, and A.R. Kay, *A method for detecting molecular transport within the cerebral ventricles of live zebrafish (*Danio rerio*) larvae*. *The Journal of physiology*, 2012. **590**(Pt 10): p. 2233-40.
44. Garcia-Lecea, M., et al., *In vivo analysis of choroid plexus morphogenesis in zebrafish*. *PLoS one*, 2008. **3**(9): p. e3090.
45. Xie, J., et al., *A novel transgenic zebrafish model for blood-brain and blood-retinal barrier development*. *BMC developmental biology*, 2010. **10**: p. 76.
46. Abbott, N.J., L. Ronnback, and E. Hansson, *Astrocyte-endothelial interactions at the blood-brain barrier*. *Nature reviews. Neuroscience*, 2006. **7**(1): p. 41-53.
47. Hori, S., et al., *A pericyte-derived angiopoietin-1 multimeric complex induces occludin gene expression in brain capillary endothelial cells through Tie-2 activation in vitro*. *Journal of neurochemistry*, 2004. **89**(2): p. 503-13.
48. Al Ahmad, A., M. Gassmann, and O.O. Ogunshola, *Involvement of oxidative stress in hypoxia-induced blood-brain barrier breakdown*. *Microvasc Res*. **84**(2): p. 222-5.
49. Engelhardt, B. and L. Sorokin, *The blood-brain and the blood-cerebrospinal fluid barriers: function and dysfunction*. *Seminars in immunopathology*, 2009. **31**(4): p. 497-511.
50. Gould, D.B., et al., *Mutations in Col4a1 cause perinatal cerebral hemorrhage and porencephaly*. *Science*, 2005. **308**(5725): p. 1167-71.
51. McCarty, J.H., et al., *Defective associations between blood vessels and brain parenchyma lead to cerebral hemorrhage in mice lacking alphaV integrins*. *Molecular and cellular biology*, 2002. **22**(21): p. 7667-77.
52. Malicki, J., et al., *Mutations affecting development of the zebrafish retina*. *Development*, 1996. **123**: p. 263-73.
53. Gross, J.M., et al., *Identification of zebrafish insertional mutants with defects in visual system development and function*. *Genetics*, 2005. **170**(1): p. 245-61.
54. Cervený, K.L., et al., *The zebrafish flotte lotte mutant reveals that the local retinal environment promotes the differentiation of proliferating precursors emerging from their stem cell niche*. *Development*. **137**(13): p. 2107-15.

55. Gregory-Evans, C.Y., et al., *Gene-specific differential response to anti-apoptotic therapies in zebrafish models of ocular coloboma*. Mol Vis. **17**: p. 1473-84.
56. Natarajan, S.K. and D.F. Becker, *Role of apoptosis-inducing factor, proline dehydrogenase, and NADPH oxidase in apoptosis and oxidative stress*. Cell health and cytoskeleton, 2012. **2012**(4): p. 11-27.
57. Kishi, S., et al., *The identification of zebrafish mutants showing alterations in senescence-associated biomarkers*. PLoS genetics, 2008. **4**(8): p. e1000152.
58. Witmer, A.N., et al., *Vascular endothelial growth factors and angiogenesis in eye disease*. Progress in retinal and eye research, 2003. **22**(1): p. 1-29.
59. Zappaterra, M.D., et al., *A comparative proteomic analysis of human and rat embryonic cerebrospinal fluid*. Journal of proteome research, 2007. **6**(9): p. 3537-48.
60. Gato, A., et al., *Analysis of cerebro-spinal fluid protein composition in early developmental stages in chick embryos*. J Exp Zool A Comp Exp Biol, 2004. **301**(4): p. 280-9.
61. Calvo-Vidal, M.N. and L. Cerchietti, *The metabolism of lymphomas*. Curr Opin Hematol.
62. Gato, A., et al., *Embryonic cerebrospinal fluid regulates neuroepithelial survival, proliferation, and neurogenesis in chick embryos*. The anatomical record. Part A, Discoveries in molecular, cellular, and evolutionary biology, 2005. **284**(1): p. 475-84.
63. Abbas, L. and T.T. Whitfield, *Nkcc1 (Slc12a2) is required for the regulation of endolymph volume in the otic vesicle and swim bladder volume in the zebrafish larva*. Development, 2009. **136**(16): p. 2837-48.
64. Smith, T.F., *Diversity of WD-repeat proteins*. Sub-cellular biochemistry, 2008. **48**: p. 20-30.
65. Thisse, B., Thisse, C. , *Fast Release Clones: A High Throughput Expression Analysis, in ZFIN Direct Data Submission (<http://zfin.org>)*. 2004. p.
66. Tian, L., et al., *Distinct acyl protein transferases and thioesterases control surface expression of calcium-activated potassium channels*. The Journal of biological chemistry, 2012. **287**(18): p. 14718-25.
67. Herring, B.E., et al., *Cornichon proteins determine the subunit composition of synaptic AMPA receptors*. Neuron. **77**(6): p. 1083-96.
68. Thisse, B., Pflumio, S., Fürthauer, M., Loppin, B., Heyer, V., Degraeve, A., Woehl, R., Lux, A., Steffan, T., Charbonnier, X.Q. and Thisse, C. , *Expression of the zebrafish genome during embryogenesis in ZFIN Direct Data Submission (<http://zfin.org>)*. 2001.

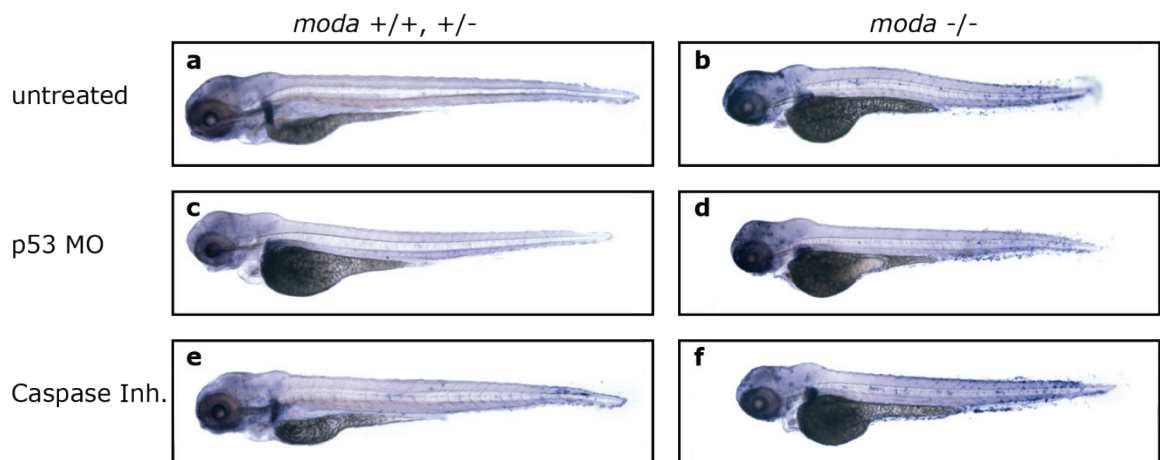
69. Taylor Clelland, C.L., et al., *Mapping and developmental expression analysis of the WD-repeat gene Preb*. Genomics, 2000. **63**(3): p. 391-9.
70. Tian, L., et al., *Distinct acyl protein transferases and thioesterases control surface expression of calcium-activated potassium channels*. J Biol Chem. **287**(18): p. 14718-25.
71. Chen, S., and Kimelman, D. , *Submission and Curation of Gene Expression Data.*, in *ZFIN Direct Data Submission (<http://zfin.org>)*. 2003.
72. Swartz, M.E., et al., *Examination of a palatogenic gene program in zebrafish*. Dev Dyn. **240**(9): p. 2204-20.
73. Bloom, L. and H.R. Horvitz, *The Caenorhabditis elegans gene unc-76 and its human homologs define a new gene family involved in axonal outgrowth and fasciculation*. Proc Natl Acad Sci U S A, 1997. **94**(7): p. 3414-9.
74. Uekita, T. and R. Sakai, *Roles of CUB domain-containing protein 1 signaling in cancer invasion and metastasis*. Cancer Sci. **102**(11): p. 1943-8.
75. Tolosano, E. and F. Altruda, *Hemopexin: structure, function, and regulation*. DNA Cell Biol, 2002. **21**(4): p. 297-306.
76. Tang, D., et al., *The ubiquitin ligase HACE1 regulates Golgi membrane dynamics during the cell cycle*. Nat Commun. **2**: p. 501.
77. Torrino, S., et al., *The E3 ubiquitin-ligase HACE1 catalyzes the ubiquitylation of active Rac1*. Dev Cell. **21**(5): p. 959-65.
78. Morita, M. and T. Imanaka, *Peroxisomal ABC transporters: structure, function and role in disease*. Biochim Biophys Acta. **1822**(9): p. 1387-96.
79. Tseng, Y.C., et al., *Specific expression and regulation of glucose transporters in zebrafish ionocytes*. Am J Physiol Regul Integr Comp Physiol, 2009. **297**(2): p. R275-90.
80. Jensen, P.J., J.D. Gitlin, and M.O. Carayannopoulos, *GLUT1 deficiency links nutrient availability and apoptosis during embryonic development*. J Biol Chem, 2006. **281**(19): p. 13382-7.
81. Sharp, T.V., et al., *The chromosome 3p21.3-encoded gene, LIMD1, is a critical tumor suppressor involved in human lung cancer development*. Proc Natl Acad Sci U S A, 2008. **105**(50): p. 19932-7.
82. Witzel, H.R., et al., *The LIM protein Ajuba restricts the second heart field progenitor pool by regulating Isl1 activity*. Dev Cell. **23**(1): p. 58-70.
83. Weber, G.J., et al., *Mutant-specific gene programs in the zebrafish*. Blood, 2005. **106**(2): p. 521-30.
84. Liongue, C., et al., *Zebrafish granulocyte colony-stimulating factor receptor signaling promotes myelopoiesis and myeloid cell migration*. Blood, 2009. **113**(11): p. 2535-46.

85. Avdesh, A., et al., *Regular care and maintenance of a zebrafish (Danio rerio) laboratory: an introduction*. Journal of visualized experiments : JoVE, 2012(69): p. e4196.
86. Rio, D.C., et al., *Purification of RNA using TRIzol (TRI reagent)*. Cold Spring Harbor protocols, 2010. **2010**(6): p. pdb prot5439.
87. Sullivan-Brown, J., M.E. Bisher, and R.D. Burdine, *Embedding, serial sectioning and staining of zebrafish embryos using JB-4 resin*. Nature protocols, 2011. **6**(1): p. 46-55.
88. Wyllie, A.H., G.J. Beattie, and A.D. Hargreaves, *Chromatin changes in apoptosis*. Histochem J, 1981. **13**(4): p. 681-92.
89. Freeman, R.S., S. Estus, and E.M. Johnson, Jr., *Analysis of cell cycle-related gene expression in postmitotic neurons: selective induction of Cyclin D1 during programmed cell death*. Neuron, 1994. **12**(2): p. 343-55.

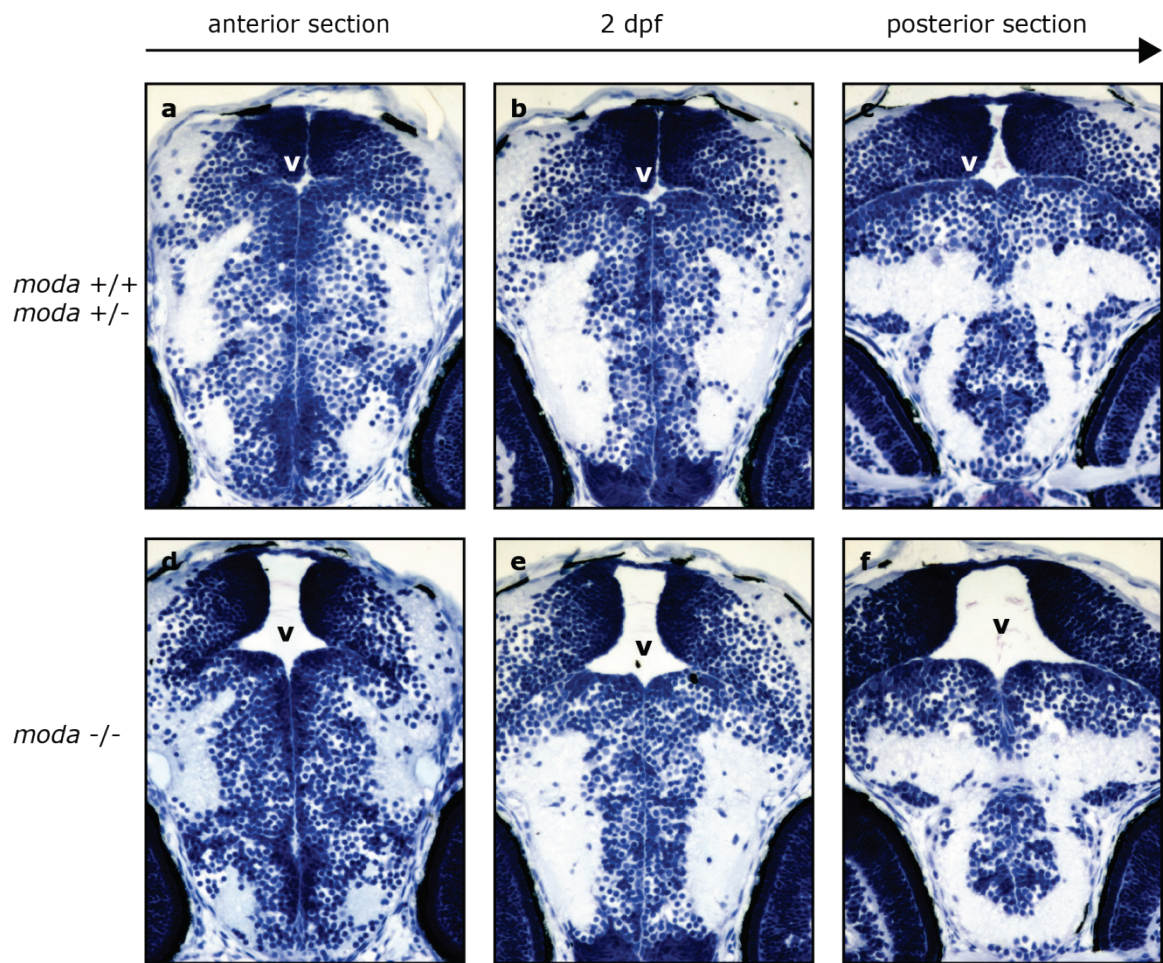
7. Annex 1: Supplementary Figures



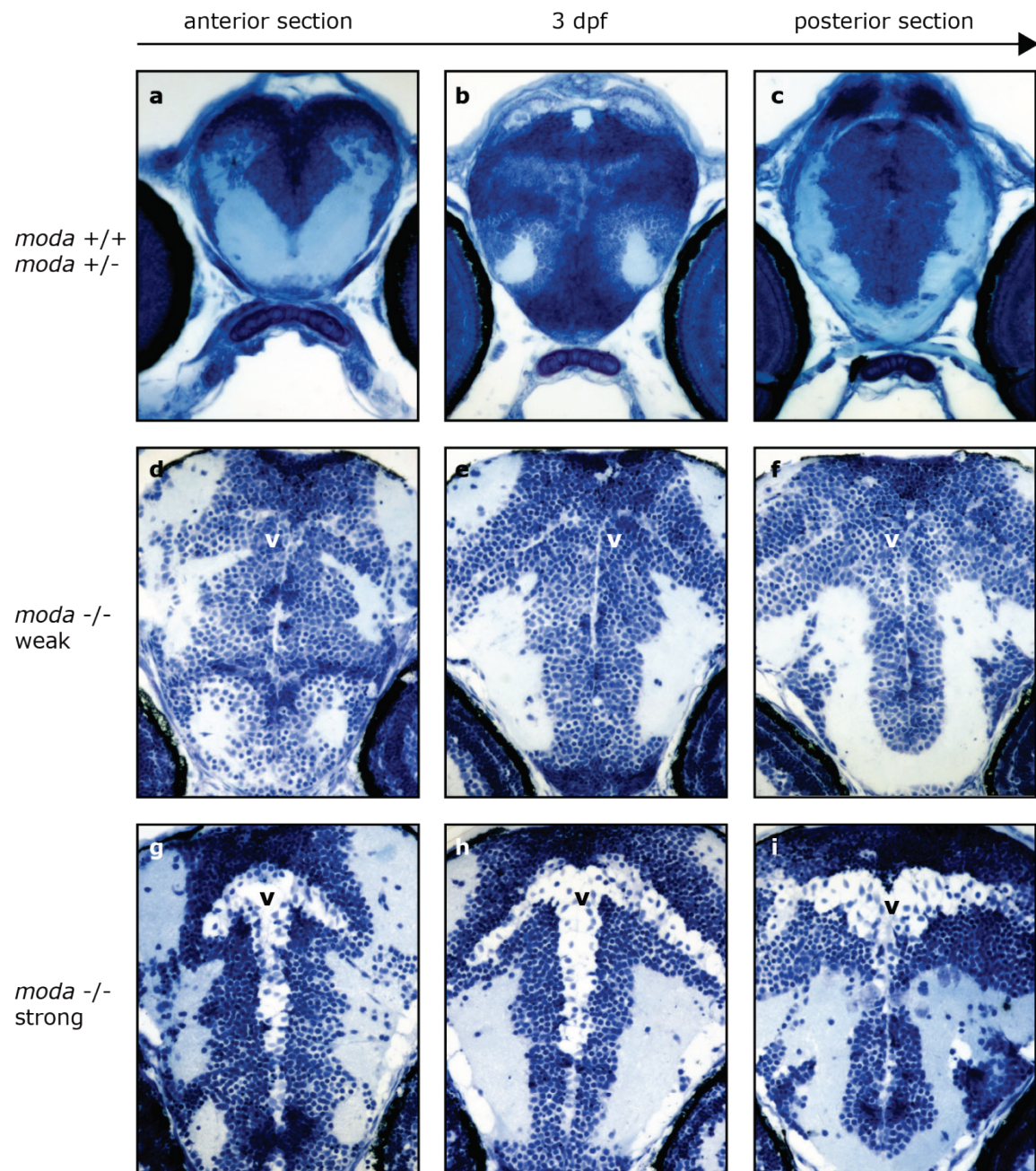
Supplementary Figure 1: The *moda* eye is unaffected until 2 dpf, when it starts degenerating from the dorsal anterior part and stretches towards the dorsal anterior surface of the brain. Serial sagittal sections of the eye stained with toluidine blue. Inserts in **g** magnify clusters of RPE cells within the stretched neural retina (yellow arrows), red arrows in **h** and **i** indicate apoptotic cell corpses.



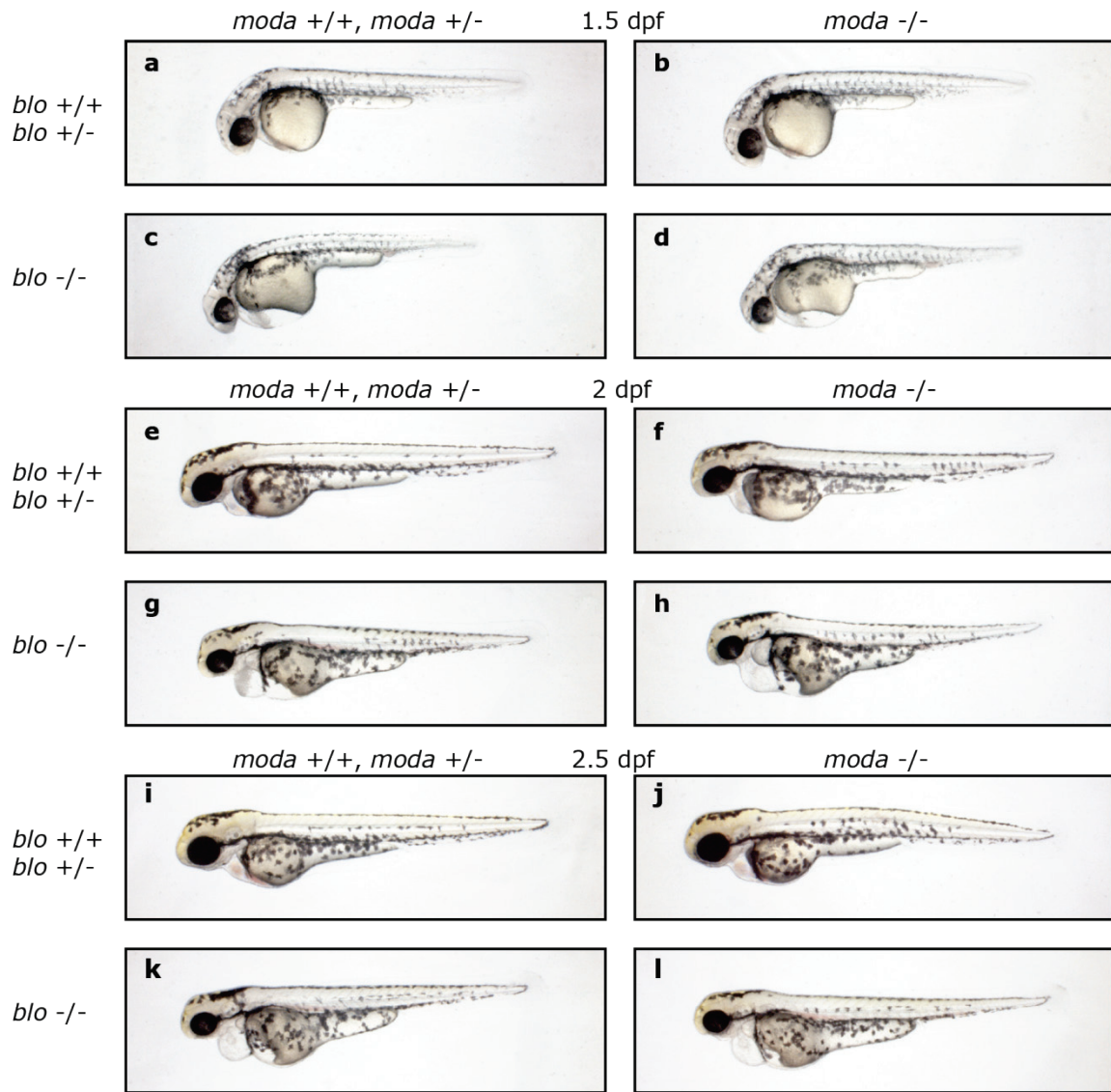
Supplementary Figure 2: Apoptosis cannot be rescued by p53MO injection and Caspase Inhibitor treatment. TUNEL staining of 3 dpf embryos. Type of treatment is indicated on the left



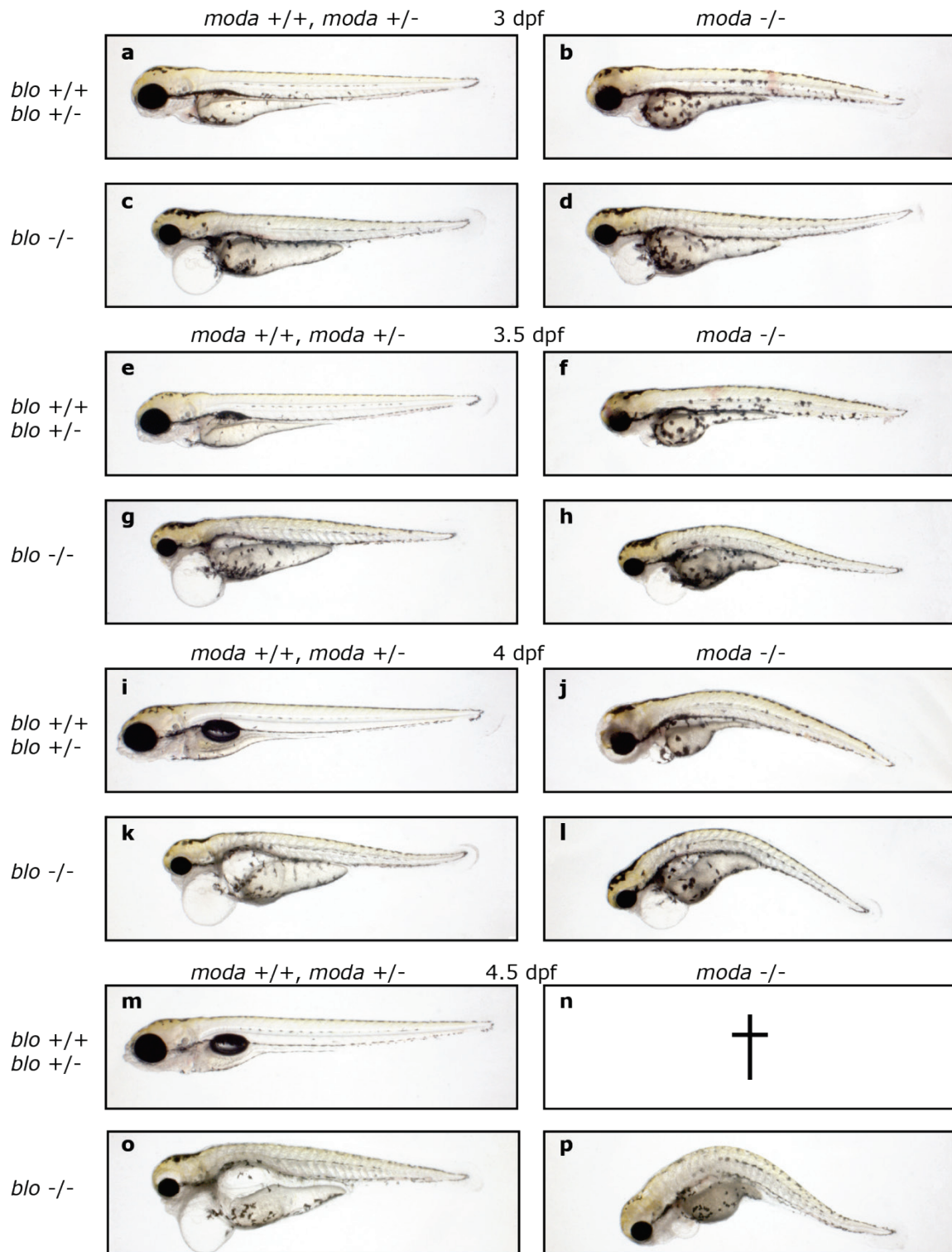
Supplementary Figure 4: Brain morphology is not affected at 2 dpf. Serial coronal sections of the brain of 2 dpf embryos stained with toluidine blue, v: ventricle



Supplementary Figure 5: The *moda* brain is severely underdeveloped at 3 dpf and shows defects along the ventricular surface. Serial coronal sections of the brain of 3 dpf embryos stained with toluidine blue, v: ventricle

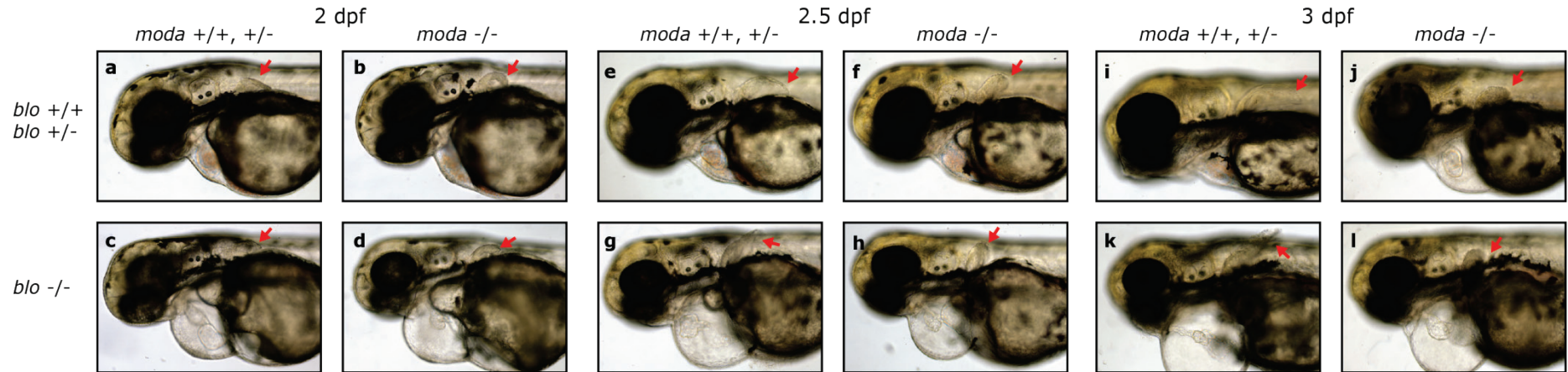


Supplementary Figure 6a: CNS degeneration is rescued in circulation deficient mutants. Live images of *blo/moda* embryos and controls at 1.5, 2 and 2.5 dpf.

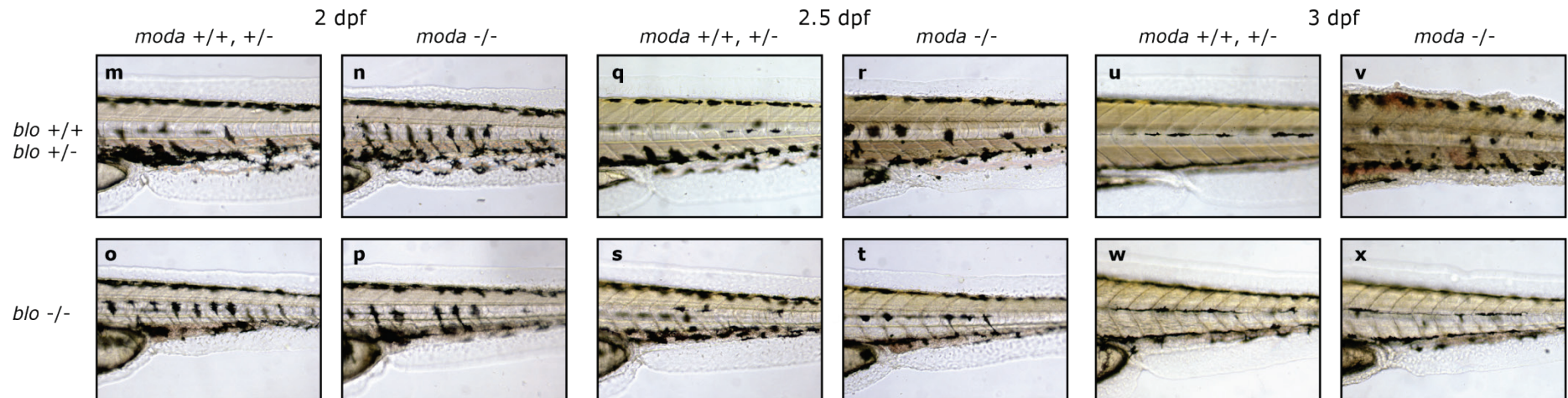


Supplementary Figure 6b: CNS degeneration is rescued in circulation deficient mutants. Live images of *blo/moda* embryos and controls at 3, 3.5, 4 and 4.5 dpf.

fin phenotype

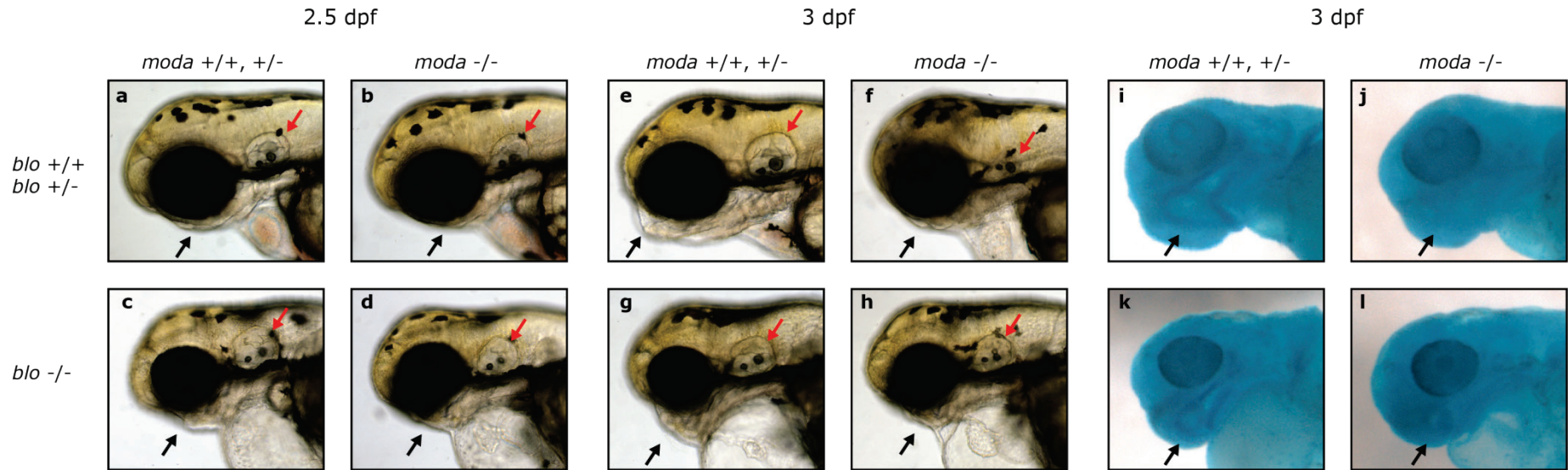


tail phenotype



Supplementary Figure 7: Live DIC images of *blo/moda* embryos highlighting the fin and tail phenotype at 2, 2.5 and 3 dpf. Tail degeneration is, but fin degeneration is not rescued in the *blo* background. Red arrows in a-l indicate the pectoral fins

jaw and otic vesicle phenotype

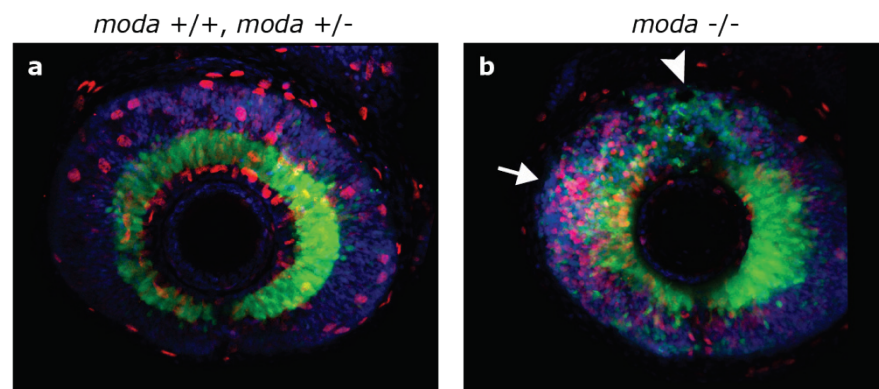


Supplementary Figure 8: Images of *blo/moda* embryos highlighting the jaw and otic vesicle phenotype. Otic vesicle collapse is, but jaw development is not rescued in the *blo* background at 3 dpf. (**a-h**) live DIC images at 2.5 and 3 dpf, (**i-l**) alcian blue staining at 3 dpf, black arrows indicate the jaws, red arrows indicate the otic vesicle

8. Annex 2: Additional observations

Cell division appears increased in the dorsal anterior part of the eye

In order to investigate cell division in the retina of *moda*, *moda* embryos were treated with BrdU at 3 dpf. In siblings cell division is restricted to the ciliary marginal zone and BrdU positive cells are distributed equally between the anterior and posterior retina. In the 3 *moda* mutants that have been analyzed cell division appears increased in the part of the eye that exhibits a slight disorganization of the RGC layer and is absent in the part that exhibits severe disorganization of the RGC layer. BrdU positive cells in the dorsal anterior eye of *moda* mutants have a morphology characteristic for apoptotic cells as they are round-shaped and strongly fluorescent^[88].



Cell division is increased in the eye of *moda* mutants at 3 dpf. Red: BrdU positive cells, green: retinal ganglion cells (*ath5:GFP* positive), blue: DAPI; white arrow indicates the area of the eye that shows a slightly disorganized RGC layer (*ath5:GFP*) and increased BrdU incorporation compared to the sibling; white arrowhead indicates the area of the eye that shows a highly disorganized RGC layer and reduced BrdU incorporation compared to the sibling.

It is rather surprising to find a high amount of BrdU incorporation in the peripheral retina, since the peripheral retina mainly contains postmitotic neurons. However, as CSF may leak from the forebrain ventricle into the developing brain and retina, the enhanced concentration of neuronal growth factors present in CSF may cause this observed increase in cell division specifically in the anterior retina. Postmitotic neurons that reenter the cell cycle often undergo apoptosis^[89], which may explain the round shaped morphology of BrdU positive cells.

9. Curriculum vitae

Name: Marion Claudia Salzer
Date of birth: 29.06.1989
Place of birth: Vienna, Austria
Nationality: Austria

Education:

2010-current: study of biology with focus on Genetics and Developmental Biology
University of Vienna
Graduation as Master of Science in July 2013

2007-2010: study of Molecular Biotechnology
University of Applied Sciences, FH Campus Wien
Graduated as Bachelor of Science

1999-2007: secondary school in Vienna, Austria

Research experience:

2011-2012: Master student in the laboratory of Dr. Stephen Wilson
University College London
research in eye development in zebrafish

2009-2011 Research technician in the laboratory of Dr. David Keays

2012-current: Institute of Molecular Pathology (IMP) Vienna
research in the molecular basis of magnetoreception in homing pigeons

Feb-Jun 2010: Bachelor student in the laboratory of Dr. Udo Bläsi
Max F. Perutz Laboratories (MFPL), Vienna
research in virulence gene regulation in *Pseudomonas aeruginosa*

Jul-Aug 2007: internship in the laboratory of Dr. Rudolph Zechner
Institute of Molecular Biosciences, University of Graz, Austria
basic research in lipometabolism

Publications:

Treiber CD, **Salzer MC**, Riegler J, Edelman N, Sugar C, Breuss M, Pichler P, Cadiou H, Saunders M, Lythgoe M, Shaw J, Keays DA; *Clusters of iron-rich cells in the upper beak of pigeons are macrophages not magnetosensitive neurons*, Nature. April 2012; 484(7394):p. 367-70

Lauwers M, Pichler P, Edelman NB, Resch GP, Ushakova L, **Salzer MC**, Heyers D, Saunders M, Shaw J, Keays DA.; *An Iron-Rich Organelle in the Cuticular Plate of Avian Hair Cells*. Curr Biol. April 2013

Braun A, Breuss M, **Salzer MC**, Flint J, Cowan NJ, Keays DA; *Tuba8 is expressed at low levels in the developing mouse and human brain*. Am J Human Genet. May 2010; 86(5): p. 819-22; author reply 822-3.

Watkins-Chow DE, Cooke J, Pidsley R, Edwards A, Slotkin R, Leeds KE, Mullen R, Baxter LL, Campbell TG, **Salzer MC**, Biondini L, Gibney G, Phan Dinh Tuy F, Chelly J, Morris HD, Riegler J, Lythgoe MF, Arkell RM, Loreni F, Flint J, Pavan WJ, Keays DA. *Mutation of the diamond-blackfan anemia gene Rps7 in mouse results in morphological and neuroanatomical phenotypes*. PLoS Genet. **9**(1): p. e1003094.

Treiber CD, **Salzer M**, Breuss M, Ushakova L, Lauwers M, Edelman N, Keays DA; *High resolution anatomical mapping confirms the absence of a magnetic sense system in the rostral upper beak of pigeons*. Communicative and Integrative Biology, April 2013, Vol.6 Issue 4

Academic writings:

Marion Claudia Salzer. Determination of the interaction sites of the sRNA PhrS and its target mRNA *pqsR* in *Pseudomonas aeruginosa*. Bachelor thesis, Max F. Perutz Laboratories, Vienna, Austria

Scholarships and certificates:

2010: Merit scholarship
2012: ERASMUS scholarship

10. Abstract/Zusammenfassung

10.1. Abstract

Congenital eye diseases are among the leading causes of blindness in developed countries. A small number of blinding diseases are caused by defects in eye development; a comparably large number are caused by defects in functional maintenance of the retina.

With the aim to identify new factors that are implicated in the maintenance of retinal integrity and function, we performed an ENU mutagenesis screen and isolated one homozygous mutant that exhibits severe retinal degeneration during late embryonic development. I termed this mutant *modern art* (*moda*). Retinal degeneration in *moda* mutants sets in at the level of the retinal pigment epithelium, a non-neural cell layer supporting the outer neural retina. Interestingly, rather than causing uniform cell death across the entire retinal tissue, the *moda* mutation leads to progressive neuronal loss primarily in the dorsal anterior quadrant of the eye.

Moda mutants display a variety of additional phenotypes. These include central nervous system (CNS) degeneration, whereby cell death starts at the ventricles and progressively spreads towards adjacent brain regions, and vascular abnormalities, which manifest in increased hemorrhaging in the CNS.

My results establish that retinal degeneration in *moda* mutants is caused by cell-extrinsic factors and that the manifestation of this phenotype is dependent on blood circulation. The mutant locus maps to a 1.4 Mb region on the left arm of Chr 16, which contains 24 candidate genes. Furthermore, I discovered that the *moda* mutation lies in a maternal effect gene. Based on my current results I suggest that cell death in the retina and CNS is caused by a disrupted neuroepithelial-ventricular barrier. Hopefully, investigation of this mutant will identify a new mechanism relevant for the pathogenesis of distinct neurodegenerative diseases in humans.

10.2 Zusammenfassung

Um unser derzeitiges Verständnis degenerativer Augenerkrankungen zu erweitern, habe ich eine neue Zebrafisch-Mutante charakterisiert, die Augendegeneration während der späten Embryonalentwicklung aufweist. Ich nannte diese Mutante *modern art (moda)*. Interessanterweise degeneriert in *moda*-Mutanten vor allem der dorsal-anterior gelegene Teil des Auges, ein Phänotyp der weder im Menschen noch in anderen Vertebraten beschrieben wurde.

Moda-Mutanten weisen eine Vielfalt zusätzlicher Phänotypen auf. Dazu gehören Degeneration des Zentralnervensystems, wobei vor allem jene Regionen betroffen sind, die sich in der Nähe des Ventrikelsystems befinden, und vaskuläre Defekte, die sich in häufigem Auftreten von Blutungen im Zentralnervensystem äußern. *Moda*-Mutanten zeigen die ersten Anzeichen von Gewebsdegeneration zwei Tage nach der Fertilisation und sterben bereits vier Tage nach der Fertilisation.

Meine Ergebnisse zeigen, dass Retina-Degeneration in *moda*-Mutanten von Zell-extrinsischen Faktoren verursacht wird und dass Blutzirkulation notwendig für die Ausprägung dieses Defekts ist. Die *moda*-Mutation liegt in einem Maternaleffekt-Gen, welches sich auf dem linken Arm von Chromosom 16 befindet.

Meine Resultate lassen vermuten, dass der massive Zelltod im Auge und Gehirn durch einen Defekt in der Barriere zwischen dem Ventrikelsystem und dem Neuroepithel verursacht wird.

11. Acknowledgements

In this last chapter of my thesis I would like to acknowledge several people who have made this work possible.

First and foremost I am very grateful to my two supervisors, Gaia and Leo, for their constant support, guidance and encouragement during all the time of research and writing this thesis. I could not have imagined having better advisors for my master's studies.

Great thanks to Steve for giving me the opportunity to work on this exciting project in his lab.

"Thanks" to Lea for having been such a great labmate and friend during my stay in London. If there would be an award for 'cheerfulness' you would be my top candidate. Thanks for bearing me companion during late weekend shifts in the lab and for the large number of beers we used to consume on Friday evenings.

"Thanks" to Pedro, Kasha, Kitti, Boie and Jing for the amazing atmosphere in our lab area and "Thanks" to all the remaining lab members for offering their help during all time.

"Thanks" to Tina Anzinger for taking me out to several electro-events and for sharing a bed with me whenever I was too tired to go the long way home to Dollis Hill.

"Thanks" to Roberto for being the most amazing housemate I could have wished for. Your pasta and chicken stew are legendary!

I would also like to thank my friends in Vienna, especially Michi for his enormous effort of reading and correcting this thesis.

And last but not least I would like to thank my family, who has supported me throughout my lifetime and has given me the opportunity to study one year abroad.